Neogene Restoration of Geometry of the Neotethyan suture zone in Central Anatolia (Turkey)

M. Özkaptan[1], E. Gülyüz[2], N. Kaymakcı[3], C. G. Langereis[4]

[1]Karadeniz Technical University, Department of Geophysical Engineering, TR-061080 Trabzon, Turkey

[2]Van Yüzüncüyıl University, Department of Geological Engineering, TR-65080 Van, Turkey

[3]Middle East Technical University, Department of Geological Engineering, TR-06800 Ankara, Turkey

[4]Utrecht University, Fort Hoofddijk Paleomagnetic Laboratory, 3584-CD Utrecht, the Netherlands

Corresponding author: Murat Özkaptan (ozkaptan@ktu.edu.tr)

Key Points:

- Excessive block rotation in Central Anatolia was revealed by paleomagnetic analysis.
- Five distinct tectonic domains were proposed in the region.
- The main factor causing these rotational differences is the deformation of the Kırşehir Block which has reigned since Neogene.

Abstract

The demise and closure of the Neotethyan Ocean gave way to the collision and finally amalgamation of various continental fragments in Turkey along the Izmir-Ankara-Erzincan and Intra-Tauride suture zones. These continental fragments include Pontides in the north and Menderes-Tauride , and Kırşehir Block in the south. This study aims to the restoration of these suture zones in central Anatolia using paleomagnetic tools during Neogene. Most of the paleomagnetic studies carried out in the region consider the deformation of Anatolian Block as a monolithic block rotated counter-clockwise due to escape tectonics since the Miocene. We introduce new paleomagnetic evidence obtained from Neogene sedimentary successions and few volcanic suits. Our results point out five distinct tectonic domains with distinct rotation patterns that indicate the rotational deformation of Central Anatolia is far more complex than generally presumed. Among these, 1) Kırıkkale-Bala Domain (KB) is rotated ~18° clockwise, 2) the Tuz Gölü Domain (TG) underwent ~15° counter-clockwise rotation, 3) the Alcı-Orhaniye Domain (AO) rotated ~25° counter-clockwise sense, 4) the Haymana Basin is divided into two different domains, (4) the Northern Haymana Domain (NHY) underwent ~17° counter-clockwise rotation while (5) the Southern Haymana Domain (SHY) underwent barely no net rotation (~5° clockwise) since the early Miocene. The Kırşehir Block was proposed to be an NNE-SSW striking tectonic block that broken into three fragments. These fragments underwent clockwise, in the north, and counterclockwise rotations in the south, respectively, during early Tertiary due to collision and N-S shortening of the Kırşehir Block between Taurides and the Pontides.

1 Introduction

Ongoing convergence between African-Eurasian and Arabian plates since at least late Cretaceous gave way to the subduction, collision, and amalgamation of various continental blocks within the Tethyan realm. In Anatolia, three continental blocks are involved in collision and amalgamation processes (Görür et al., 1984; Kaymakcı et al., 2009, 2003a, 2003b; Lefebvre et al., 2013). These include the Pontides in the north with Eurasian affinity, the Menderes-Tauride Block with Gondwana affinity in the south, and the Kırşehir Block located in between these blocks, during much of Mesozoic and early Tertiary (Kaymakcı et al., 2001) (Figure 1). Collision and further convergence of these blocks gave way to the development of İzmir-Ankara (İASZ) between Pontides and Menderes Tauride Block, Ankara-Erzincan Suture Zone (AESZ) between Pontides and the Kırşehir Block and Intra-Tauride Suture Zone (ITSZ) between Kırşehir Block and the Menderes-Tauride Block.

The active convergence between Africa and Anatolia is accommodated by northward subducting African slabs along Mediterranean trenches (e.g. Pliny-Strabo, Hellenic, and Cyprian trenches) (e.g., Le Pichon and Angelier, 1979; van Hinsbergen et al., 2010; Biryol et al. 2011). The slab-edge processes along this subduction system gave way to the development of backarc extension in the Aegean-west Anatolian region. In contrast, collision and ongoing convergence between Eurasian and Arabian plates resulted in the development of compressional deformation and N-S shortening in eastern Anatolia-Iranian Plateau region, which ultimately gave way to the westward escape of Anatolian Block Along the dextral North Anatolian and sinistral East Anatolian fault zones towards the free face of the Hellenic trench by the late Miocene (Burke and Şengör, 1986; Flerit et al., 2004; Gülyüz et al., 2019; Hüsing et al., 2009; Şengör et al., 1985).

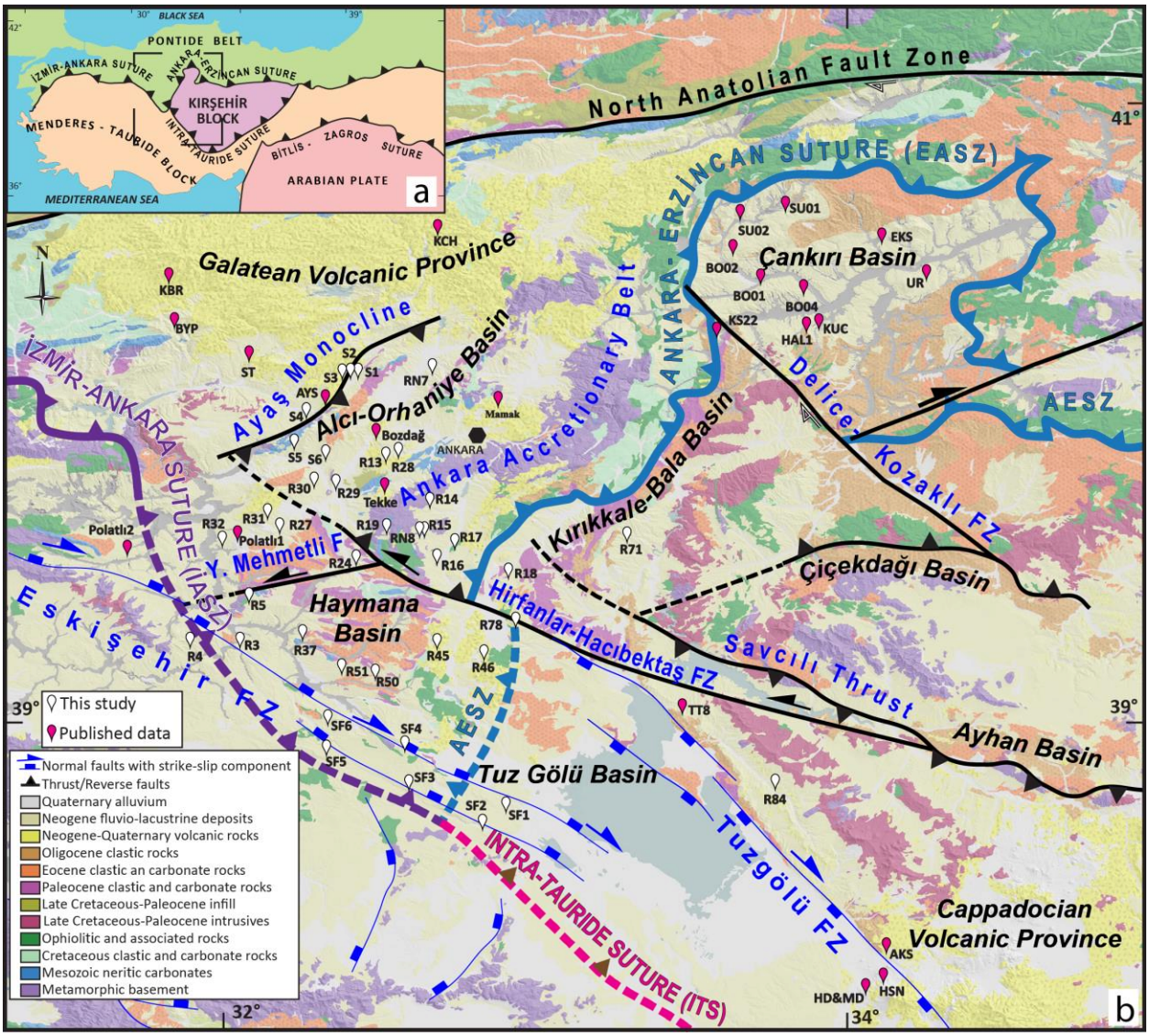

Figure 1. a) Major tectonic divisions of Anatolia (Kaymakcı et al. 2009). b) Simplified geological map (Işıker 2002) of the study area and sample locations.

Relatively recent seismotectonic (e.g. Armijo et al., 1999; Hubert-Ferrari et al., 2002; Şengör et al., 2005), Global Navigation Satellite Sytems (GNSS) (e.g. Reilinger et al., 2006) and paleomagnetic studies (Kissel et al., 1993, 1987; Tatar et al., 1995; Gürsoy et al., 1998; 1999; 2003; 2011; Piper et al., 1996;1997; 2010; Kaymakcı et al., 2007; Çinku, 2016, 2017; Hisarlı et al., 2016) studies support the escape tectonics model, and almost all of these studies claimed that the Anatolian Block had been rotated counter-clockwise since Miocene Miocene. These studies generally assume that (i) the Anatolian Block is a single homogeneous body fleeing westwards along crustal-scale faults (NAFZ and EAFZ) and stretched by slab-pull related extension along the Hellenic Trench and (ii) Miocene and younger vertical block rotations are related only to the still active transcurrent tectonics, “the Neotectonic Period,” while pre-late Miocene tectonics - covering the complete closure of Neotethys ocean in the region- is considered as “Paleotectonic Period” which is an independent deformation period prior to the Arabian collision. These studies, however, cannot explain the continuous deformation since Oligocene and onwards and related

vertical block rotations (Kaymakci et al., 2003; 2007; 2018; van Hinsbergen et al., 2005; 2010; Meijers et al., 2010; Uzel et al. 2015; 2020; Koç et al., 2016; 2017; Lefebvre et al., 2013;). Similarly, recent paleomagnetic studies from western and southwestern Anatolia demonstrated that the rotational deformation of Anatolian Block is not uniform, and it is far more complex than presumed previously. Some of these studies include Thrace Fault (Kaymakcı et al., 2007), İzmir- Balıkesir Transfer Zone (Uzel et al., 2020, 2017, 2015) Central Tauride Oroclinal Bending (Koç et al., 2016), SW Anatolian rotation (Kaymakcı et al., 2018; Özkaptan et al., 2014). Each of these studies documents heterogeneous vertical block rotation patterns continuous from Early Miocene to recent. The similarly heterogeneous deformation pattern that took place since early Miocene is also valid for Central Anatolia. In this regard, the main purpose of this paper is to demonstrate how continuous rotational deformation in Central Anatolia, since at least early Miocene, shaped the present complex geometries of İzmir-Ankara and Intra-Tauride suture zones that are related to the closure of the Neotethys Ocean and the collision of intervening continental blocks. The Central Anatolian region has been exposed to progressive compressional deformation since at least Late Paleocene by the beginning of collision between Pontides and the Kırşehir Block (Advokaat et al., 2014; Gülyüz et al., 2013; Kaymakcı et al., 2009; van Hinsbergen et al., 2016) which have led to heterogeneous and non-orthogonal deformation in the region. Our study is based on vertical block rotation restorations of post-Oligocene units based on paleomagnetic results collected from 39 new sites and reliable literature data (Table 1, Fig. 1).

2 Materials and Methods

2.1 Stratigraphy

In the literature, sedimentary sequences in Central Anatolia are classified as pre-early Miocene paleotectonic units that represent the sequences related to the closure of the Neotethys ocean and collision of intervening continental units. They are categorized as Late Cretaceous to Oligocene fore-arc to foreland basin deposits (Görür et al., 1984; 1998; Gülyüz et al., 2019, 2013; Kaymakcı et al., 2009; Koçyiğit, 1991). The second group comprises post- late Miocene continental fluvio-lacustrine sequences that are classified as Neotectonic units (Kaymakcı et al., 2001; Koçyigit, 1991; Şengör et al., 1985) deposited by the beginning of transcurrent tectonics related to the westward escape of Anatolian Block and they are the main concern of this study.

The Neotectonic units seem to unconformably overlay the paleotectonic units almost everywhere in Turkey, although the ages of most of these units are in places poorly constrained. In most cases, the first unit unconformably overlying the so-called Paleotectonic units are regarded as late Miocene, and the age of the sequence is ascribed recursively without providing any biostratigraphic or radiometric evidence (e.g. Koçyiğit, 1991; Koçyiğit et al., 1995). In order to overcome such a limitation, the ages of the studied sections in this study are based on available biostratigraphic and radiometric data wherever available otherwise we followed the ages proposed by the Geological Survey of Turkey (Işıker, 2002). The sampled horizons, in this study, range from Oligocene to Early Quaternary and they can be traced over more than 100 km distance, especially in the Haymana and Tuzgölü basins, making lateral correlations straightforward and reliable (Fig. 1, Table 1). In the Alcı-Orhaniye and Çankırı basins, biostratigraphic data is adequately abundant (Saraç, 2003), which provided better constraints on the ages of the sampled units (Fig. 1).

2.2 Geological Setting

The tectonic elements in the study area include various basins and major faults and faults that controlled the rotation deformation of the region. Among these, Haymana Basin, Kırıkkale-Bala Basin, Tuzgölü Basin, Alcı-Orhaniye Basin and Çankırı Basin are very important in term of hosting Neogene deposits from which sampling was carried out.

The Haymana Basin is located at the southernmost tip of the Central Pontides and straddles the İzmir-Ankara Suture Zone in the north NW part of the Intra-Tauride Suture Zone (Fig. 1). The Neogene structures affecting the basin are the Eskişehir Fault Zone (EFZ) in the south and the Dereköy Fault (DF) in the north. The Derekeköy Fault is a reverse fault zone which reactivated as a sinistral strike-slip fault zone with reverse component during the Neogene. It is the northwestern continuation of the Hirfanlar-Hacıbektaş Fault Zone of Lefebvre et al. (2013) and Özkaptan and Gülyüz (2019). Gülyüz et al. (2019) have documented kinematic data on two newly recognized NE-SW striking Neogene strike-slip faults that segmented and controlled the deformation in the Haymana Basin.

The Çankırı and Kırıkkale-Bala basins are fore-arc to fore-land basins that straddle the Ankara-Erzincan Suture Zone (Fig. 1) and their Tertiary (foreland basin) configuration sandwiched between the Pontides and Kırşehir Block (Kaymakcı et al., 2009). The main structures that controlled the Neogene tectonics of the Kırıkkale-Bala Basin are the Tuz Gölü Fault, Delice-Kozaklı and Hacılar-Hirfanlı Fault zones (Gülyüz et al., 2013; Lefebvre et al., 2013).

The Tuz Gölü Basin straddles the Intra-Tauride Suture Zone and is located both on the Kırşehir and the Tauride blocks. Its Neogene evolution is dominated by the Tuz Gölü Fault Zone along its eastern margin and Eskişehir Fault Zone along the western margin (Çemen et al., 1999). The Alcı-Orhaniye Basin is located within the Pontides and bounded in the east by the basement rocks of the Pontides exposed within the Ankara Accretionary Belt (Rojay, 2013). In the west, the Ayaş Monocline - an inverted normal fault reactivated as a west verging reverse fault, delimits the basin.

Two major magmatic complexes emplaced mainly during the Neogene dominate the tectono-magmatic evolution of the region. The Galatian Volcanic Province (GVC, Tankut et al., 1999) is developed within the Pontide Block at the NW part of the study area, and the Cappadocia Volcanic Province (CVC, Toprak, 1998) is developed within the Kırşehir Block in the SE part of the basin. The origin of the GVC is attributed to post-collisional magmatic processes along the İzmir-Ankara Suture Zone (Kaymakcı et al., 2009) whereas the origin of CVC is attributed to the Mediterranean subduction systems (Di Giuseppe et al., 2018; Toprak, 1998, 1994).

3 Paleomagnetism and rock magnetism

3.1 Paleomagnetic sampling

We have carried out an extensive paleomagnetic sampling campaign and collected more than 900 standard paleomagnetic core samples (25 mm Ø) from 39 different sites comprising Miocene to Pliocene sedimentary sequences (Fig. 1 and Table 1). The sampling was performed using a gasoline-powered drill or using a portable generator and an electric drill. At least 6 but generally more than 15 (up to 46) oriented core samples were collected at each site, over 5 to 15 meters stratigraphic thickness to average out paleosecular variation (PSV). In addition to sedimentary sites, three igneous sites (R13, R45, R46) were sampled, each consisting of at least

7 different cooling levels (lava flows). The sedimentary sites are composed of Miocene shale/ silty clay, marl and limestone, and Pliocene mudstone/marl and limestone. The igneous sites are composed of andesitic and basaltic lava flows. Core orientations and bedding planes were measured with a magnetic compass which was corrected for the present-day declination (+4.5°E, 2013). The preparation of the samples, as well as demagnetization and rock magnetic experiments, were carried out at the Fort Hoofddijk Paleomagnetic Laboratory at Utrecht University (the Netherlands).

3.2 Demagnetization procedures

The paleomagnetic samples were cut into standard specimens (2.2 cm in length), per core sample usually resulting in several specimens (referred to as A, B) providing the opportunity to compare single core results. Natural remanent magnetizations (NRM) were analyzed by applying both thermal (TH) and alternating field (AF) stepwise demagnetization. A total of 976 specimens were demagnetized. At least 5 specimens per site were thermally demagnetized. The demagnetization started from room temperature (20°C) and went up to a maximum of 680°C (using 20-50°C steps). The TH demagnetization was carried out in a magnetically shielded oven (ASC, model TD48-SC) with a residual magnetic field < 10 nT. Specimens were measured on a 2G Enterprises horizontal 2G DC SQUID cryogenic magnetometer (noise level 3×10^{-12} Am^2).

In addition, on average 6 specimens per site were heated to 150°C before AF demagnetization to remove possible stress in magnetite due to low-temperature oxidation (weathering) (Van Velzen and Zijderveld, 1995). The rest of the specimens were only AF demagnetized, carried out with increments of 3–10 mT up to a maximum of 100 mT. AF demagnetization was done using an in-house developed robotized 2G Enterprises DC SQUID cryogenic magnetometer (noise level $1\text{-}2\times10^{-12}$ Am^2) in a magnetically shielded room (Mullender et al., 2016).

3.3 Thermomagnetic experiments

In order to determine the nature of the dominant magnetic carrier(s) in the studied rocks and their alterations under different temperatures, thermomagnetic experiments were carried out on at least one specimen per site. Representative results of 15 specimens of different rock types and ages are illustrated in Figure 2. Curie balance runs were carried out in the air, using a modified horizontal translation type Curie balance with a sensitivity of ~5x10-9 Am^2 (Mullender et al., 1993). Approximately 0.3-0.9 g of powdered rock sample was put into a quartz-glass sample holder and measured in a number of heating-cooling cycles (with rates of 10°C /min) in air, up to a maximum temperature of 700°C. We used the following heating-cooling cycles (in $^{\circ}$C): 20–150, 50–250, 150–350, 250–400, 300–450, 350–525, 420–580, and 500–700.

3.4 Paleomagnetic analysis

The directional and statistical results were analyzed using the online portal Paleomagnetism.org (Koymans et al., 2016). The demagnetization results from AF, TH and combined measurements were by orthogonal projection diagrams (Zijderveld, 1967) (Fig. 3). Characteristic Remanent Magnetization (ChRM) directions were determined using principal component analysis following an eigenvector approach (Kirschvink, 1980) by taking approximately five to seven vector points. Interpreted directions are plotted in equal-area projections (Fig. 4). In the case of two or more overlapping coercivity or temperature components, ChRM directions were determined by following the great circle approach of

McFadden and McElhinny (1988) (Fig. 3). The means of both ChRM directions and their corresponding virtual geomagnetic poles (VGP) were computed using Fisher (1953) statistics. We used the Deenen et al. (2011, 2014) criteria to test for sufficiently averaging out paleosecular variation (PSV), by calculating the A95 of the VGP distribution. If A95 is within the N-dependent range (between A_{95min} and A_{95max}), it may be assumed that the rocks have recorded PSV. We applied a fixed cut-off (45°) to remove outliers, following Deenen et al. (2011). The errors in declination (ΔD_x) and inclination (ΔI_x) were determined from A95 of the VGP distribution (according to Butler, 1992; see also Deenen et al. 2011). To determine whether two distributions share a common true mean direction (CTMD), we used the coordinate bootstrap test (Tauxe, 2010; Fig. 5).

4 Rock magnetism, NRM properties and Paleomagnetic results

4.1 Rock magnetism

Thermomagnetic experiments were implemented for every site of which we selected 2 volcanic and 13 sedimentary rocks. Representative diagrams from five different localities are given in Fig. 2. Two types of thermomagnetic curves can be observed in the volcanic sites. Site R13 (andesite) dominated by magnetite since the major decay occurs at ˜575°C (Fig. 2g), while some magnetization is lost above 350°C, pointing to some maghemite possibly due to low-temperature oxidation (weathering). Site R45 shows a sharp decrease in magnetization with a Curie temperature around 300 °C which suggests the presence of Ti-rich titanomagnetite as the dominant magnetic carrier (Fig. 2m). A second Curie temperature of ˜550-580°C supports the presence of Ti-poor magnetite as well. Most sedimentary sites show Curie temperatures of ˜550-580°C pointing to magnetite as the main carrier of the NRM. In many cases, the curves show that some magnetization is lost at temperatures above ˜350°C, but usually, cooling curves become reversible again above 450-500°C which suggests the presence of some maghemite in the samples that at ˜350°C may invert to hematite and thus the sample becomes less magnetic (Dankers, 1978). Generally, lake sediments present relatively low magnetizations and the curves suggest the dominant presence of paramagnetic minerals (e.g. Fig. 2h, i). Nevertheless, in most cases, in both volcanics and sediments, the main magnetic carrier of the ChRM is magnetite, as determined by the Curie temperatures of ˜580°C. Only a small number of samples survive up to ˜650-680°C, indicating the presence of hematite.

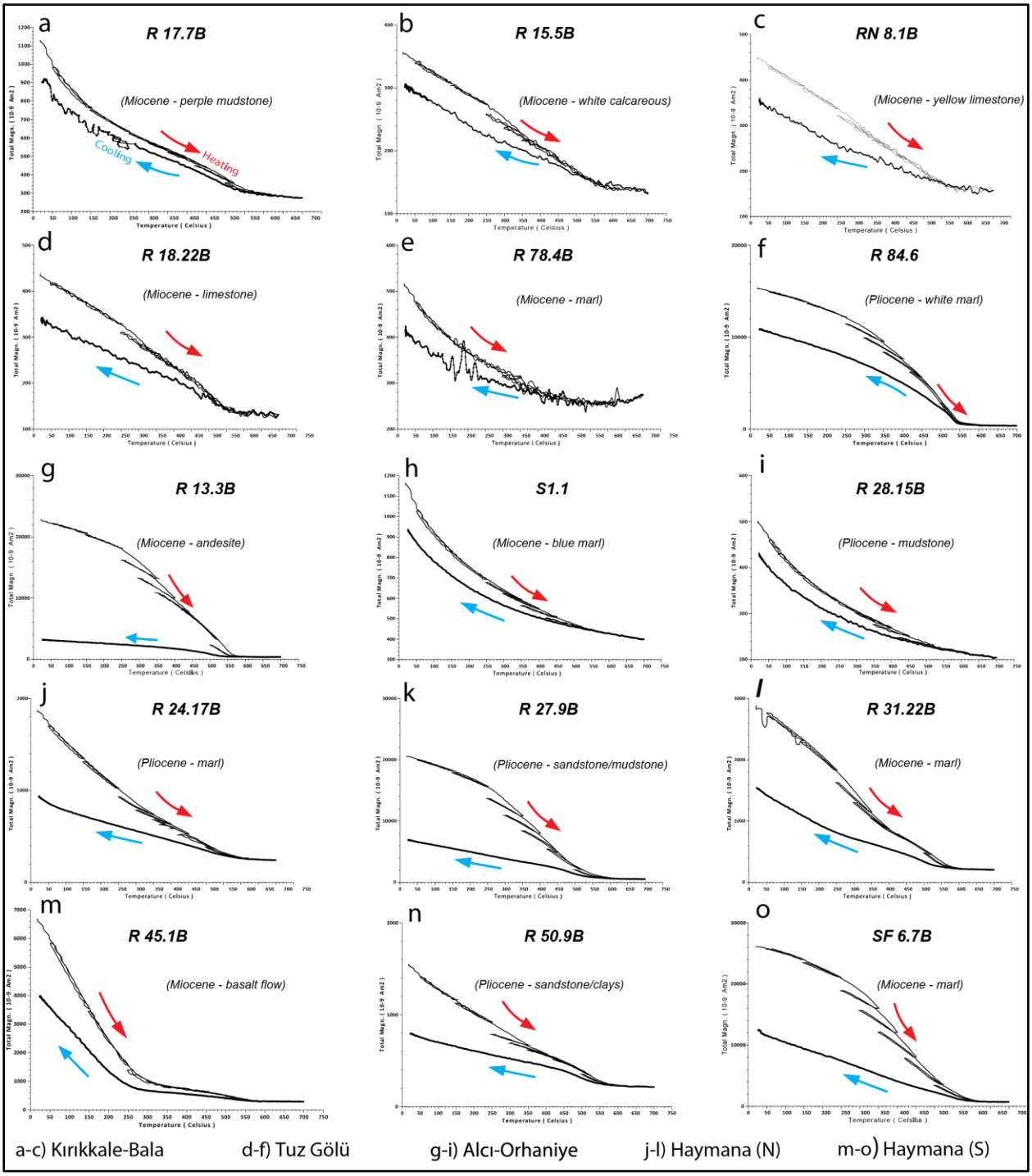

Figure 2. Thermomagnetic (cure-balance) curve generated with the stepwise heating protocol (Mullender et al., 1993) for 18 representative samples in five different domains in Central Anatolia. The thin black line (red arrow) shows heating phases. The final cooling segment is indicated with thicker black line (blue arrow). A noisy appearance is indicative of a weak magnetic signal. Detailed explanations are given in the text.

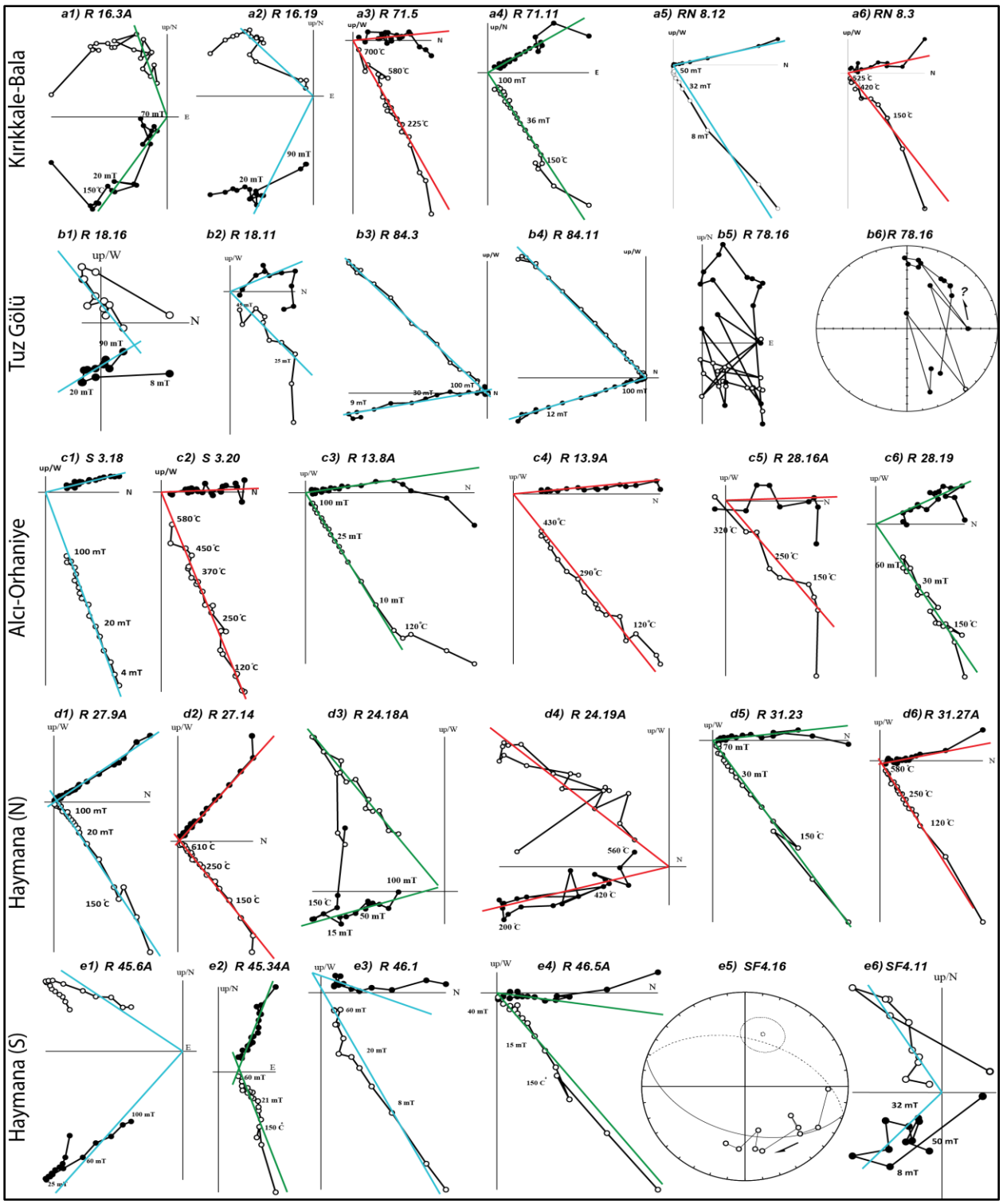

Figure 3. Zijderveld diagrams (Zijderveld, 1967) of representative samples at five domains demagnetized using thermal (red lines, TH), alternating field (blue lines, AF), and preheated alternating field (green lines, TH-AF) demagnetization shown in tectonic coordinates. The solid and open dots represent projections on the horizontal and vertical planes, respectively. Great circle plots (b6, e5) use the technique of McFadden and McElhinny (1988). Demagnetization step values are in ^{o}C, in mT, or both.

4.2 NRM properties

Small viscous remanent magnetization components with a random direction are usually removed at low temperatures (100-120°C) or low alternating fields (4-15mT) while a recent magnetic field overprint – if at all present - could be removed at ˜180-220°C. In a few specimens, we suspect the presence of some greigite, which has relatively high coercivity but low Curie temperatures of 320-350°C. Greigite can be dominant in many Neogene sediments in the southern Eurasian basins but still can provide reliable results (Özkaptan et al., 2018; Vasiliev et al., 2008). In most cases, however, the maximum temperatures required to remove the ChRM entirely are close to ˜580°C or 80-100 mT and point again to magnetite as the main carrier of the NRM. Occasionally, higher temperatures or alternating fields above 100 mT are required in which case we must have hematite. Relevant examples are shown in Fig. 3.

Based on the accepted sites and using relevant literature data, the region was divided into five main domains, based on rotation patterns and geological characteristics. Initially, the statistical results were analyzed on a site by site basis, and subsequently, all directions of each site were combined for each domain to give the mean rotation result per locality (Table 1, Fig. 4). We discerned five localities, namely: Kırıkkale-Bala (KB), Tuz Gölü (TG), Alcı-Orhaniye (AO), Haymana (NHY), and Haymana (SHY).

5 Paleomagnetic results

5.1 Kırıkkale-Bala (KB)

This domain comprises Kırıkkale-Bala Basin and associated areas. We have collected 150 samples from 7 Upper Miocene-Pliocene sites from the domain. Among these, 84 of them are measured, and remaining ones are kept as a backup (Table 1). Two out of seven sites were disregarded since they did not produce any meaningful results. The site R14 produced random directions, and R15 most probably was effected by lightening. The remaining 5 sites show both normal (R71 and RN8) and reversed (R 16, R 17, and R 19) polarities. The normal polarity sites belong to Upper Miocene – Pliocene sequences and indicate no significant rotations (D = 1.1 ± 12.5°) after tilt correction. However, the three reversed polarity sites belong to Upper Miocene sequences and all indicate a similar sense of declination having a mean direction of 19.9 ± 4.7° with CW sense rotation. The reversed polarity site mean inclination (I = 41.3 ± 5.8°) is lower than the expected inclination (I = ~57.5°, Ankara), possibly due to inclination shallowing related to compaction of the sediment, whereas the normal site mean has a steep inclination (I = 62.4 ± 7.4°) after tilt correction. This inclination before tilt correction (I = 52.5 ± 8.6°) is not significantly different from the expected inclination at this latitude and therefore possibly caused by a recent field overprint that was not sufficiently removed. An alternative explanation would be due to termination of rotational deformation towards the end of Miocene or possibly during Pliocene. However, the reversal test between the mean normal and reversed results is negative (Fig. 5). We, therefore, retain only the mean of the reversed sites providing a 19.9 ± 4.7° CW rotation for the Upper Miocene rocks of the Kırıkkale-Bala Domain (Table 1).

Table 1. Paleomagnetic results presented in this study and localities parametrically resampled from previous studies. Lat/Long (°): the latitude and longitude of sites and localities, Nc: number of samples collected, N_m: number of samples measured, N_{45}: number of samples after application of a fixed cutoff (45°), Dec: declination, Inc: inclination, ΔD: declination error, ΔI: inclination error, k: estimate of the precision parameter determined from the ChRM directions, α95: cone of confidence determined from the ChRM directions, K: precision parameter determined from the mean virtual geomagnetic pole (VGP) directions, A95: cone of confidence of the mean virtual geomagnetic pole (VGP). $A95_{min}$ and $A95_{max}$ represent the confidence envelope of Deenen et al. (2011). If A95 falls within this envelope the distribution likely represents paleosecular variation. All site and domain results are given in both in-situ and tilt adjusted depending on our interpretation as explained in the text.

Site/Locality	*Lat. (N°)*	*Long. (E°)*	*Age*	*MN Zones*	*Nc*	*ChRM Directions (in situ)*							*ChRM directions (tilt adjusted)*									
						N_m/N_{45}	*Dec*	*ΔD*	*Inc*	ΔI_x	*k*	*a95*	*Dec*	*ΔD*	*Inc*	*ΔI*	*k*	*a95*	*K*	*λ*	$A95_{min}$	*A95*	$A95_{max}$
Kırıkkale-Bala (Upper Miocene-Pliocene)																						
~~R 14~~	39.69085°	32.68084°	Upper Miocene	MN9-12	14	12 / 00	No reliable result															
~~R 15~~	39.59717°	32.66710°	Upper Miocene	MN9-13	28	11 / 00	No reliable result (Lightning)															
R 16	39.50370°	32.74693°	Upper Miocene	MN9-14	29	18 / 16	199.0	07.2	-40.4	09.6	026.8	07.3	198.0	06.3	-27.5	10.2	026.8	07.3	038.0	-14.6	04.0	06.1	14.3
R 17	39.55369°	32.82139°	Upper Miocene	MN9-15	21	20 / 18	195.1	08.0	-26.7	13.2	018.3	07.8	212.6	07.8	-43.7	09.0	031.2	06.3	025.4	-25.5	03.8	07.0	13.3
R 19	39.61479°	32.52476°	Upper Miocene	MN9-15	27	23 / 23	193.0	06.9	-48.4	07.0	034.1	05.3							026.3	-29.4	03.4	06.0	11.4
R 71	39.55996°	33.30906°	U. Mio-Plio.	MN9-15	18	17 / 15	003.9	14.5	56.6	11.0	019.6	08.9	014.8	18.5	64.6	09.8	019.6	08.9	010.1	46.5	04.1	12.6	14.9
RN8	39.59717°	32.66710°	U. Mio-Plio.	MN9-15	13	11 / 09	356.5	11.8	45.5	13.0	025.2	10.5	350.4	15.9	57.6	11.5	025.2	10.5	018.2	38.2	05.0	12.4	20.5
Mean (N)						**24 / 24**	**000.7**	**09.7**	52.5	**08.6**	**020.0**	**06.8**	001.1	**12.5**	62.4	**07.4**	**021.9**	**06.6**	**012.3**	**43.7**	**03.4**	**09.0**	**11.4**
Mean (R)						**60 / 58**	**196.2**	**04.3**	-38.8	**05.6**	**020.3**	**04.2**	199.9	**04.7**	-41.3	**05.8**	**020.2**	**04.3**	**019.9**	**-23.7**	**02.4**	**04.3**	**06.4**
Mean (N+R)						**84 / 79**	**011.9**	**04.4**	**43.1**	**05.2**	**016.9**	**03.9**	**018.0**	**04.9**	**46.6**	**05.3**	**016.5**	**04.0**	**014.4**	**27.9**	**02.1**	**04.3**	**05.2**
Tuz Gölü (Oligo.-Mio.-Pliocene)																						
TT8*	38.97973°	33.50288°	Oligo-Miocene		8	8/8	344.5	08.4	47.4	08.7	059.4	07.2	327.0	12.9	60.5	08.3	059.4	07.2	034.2	41.5	05.2	09.6	22.1
R 18	39.44065°	32.93658°	Middle Miocene	MN6-8	33	24 / 24	355.0	11.6	56.1	09.0	017.4	07.3	351.3	08.5	42.4	10.2	017.4	07.3	015.5	24.6	03.4	07.8	11.1
~~R 78~~	39.31113°	32.93993°	Upper Miocene	MN9-12	20	15 / 00	No reliable result															
R 84	38.75762°	33.79107°	U. Mio-Plio.	MN9-15	28	24 / 24	164.4	02.9	-49.4	02.8	200.1	02.1							143.2	-30.3	03.4	02.5	11.1
Mean (N+R)						**56/56**	**347.5**	**04.8**	**51.7**	**04.3**	**035.0**	**03.3**	**345.8**	**04.7**	**48.3**	**04.8**	**026.8**	**03.7**	**022.1**	**29.3**	**02.4**	**04.1**	**06.5**
Alcı-Orhaniye (Miocene)																						
S 1	40.09339°	32.43849°	Upper Miocene	MN9-12	24	23/23	346.8	07.9	60.1	05.2	046.7	04.5	331.9	05.4	45.8	05.9	046.7	04.5	040.7	27.2	03.4	04.8	11.4
~~S 2~~	40.09537°	32.42591°	Upper Miocene	MN9-12	6	2/1	No reliable result															
S 5	39.87782°	32.22427°	Upper Miocene	MN9-12	28	20 / 16	165.2	06.5	-11.3	12.6	027.4	07.2	162.2	07.7	-34.3	11.1	027.4	07.2	026.7	-18.8	04.0	07.3	14.3
~~S 6~~	39.81832°	32.33579°	Upper Miocene	MN9-12	39	20 / 20	351.9	06.3	53.0	05.4	056.7	04.4	301.0	05.1	40.7	06.4	056.7	04.4	049.1	23.3	03.6	04.7	12.4
RN 7	40.10062°	32.67606°	Upper Miocene	MN9-12	19	21 / 10	337.6	22.2	61.1	13.8	018.4	11.6	324.2	10.4	31.3	15.8	018.4	11.6	024.7	16.9	04.8	09.9	19.2
R 30	39.75496°	32.32426°	Upper Miocene	MN9-12	19	19 / 13	176.0	10.1	-37.8	13.6	018.4	09.9	149.3	09.5	-36.4	13.1	018.4	09.9	022.5	-20.2	04.3	08.9	16.3
Mean (N)						**33 / 33**	**344.1**	**08.1**	**60.5**	**05.3**	**032.6**	**04.4**	**329.2**	**05.0**	**41.6**	**06.2**	**026.5**	**05.0**	**030.4**	**23.9**	**03.0**	**04.6**	**09.1**
Mean (R)						**29 / 29**	**169.4**	**06.4**	**-23.2**	**11.1**	**013.8**	**07.5**	**156.5**	**06.2**	**-35.4**	**08.7**	**021.2**	**05.9**	**022.2**	**-19.5**	**03.1**	**05.9**	**09.8**
Mean (N+R)						**61 / 62**	**347.0**	**05.8**	**42.9**	**06.8**	**011.0**	**05.8**	**332.4**	**04.0**	**39.1**	**05.2**	**023.2**	**03.9**	**025.2**	**22.1**	**02.3**	**03.7**	**06.2**
Alcı-Orhaniye (Pliocene)																						
~~S 3~~	40.10604°	32.40219°	Pliocene	MN15	27	20 / 19	356.5	05.1	51.0	04.8	085.2	03.8	355.8	13.0	74.0	04.0	085.2	03.8	029.7	60.1	03.8	06.4	13.3
S 4	39.99441°	32.28423°	Pliocene	MN15	24	13 / 13	005.7	23.0	68.8	09.6	023.8	08.7	326.5	10.4	48.2	10.6	023.8	08.7	021.9	29.2	04.3	09.1	16.3
R 28	39.85070°	32.60247°	Pliocene	MN15	26	17 / 17	335.8	09.9	57.6	07.2	037.7	05.9	346.4	06.2	37.7	08.3	037.7	05.9	039.0	21.1	03.9	05.8	13.8
R 29	39.73686°	32.37431°	Pliocene	MN15	18	17 / 13	335.0	11.0	50.7	10.3	026.6	08.2							020.5	31.5	04.3	09.4	16.3
Mean (N)						**43 / 43**	**339.9**	**07.2**	**57.3**	**05.3**	**027.3**	**04.4**	**337.7**	**05.5**	**45.1**	**06.2**	**023.1**	**04.6**	**020.5**	**26.6**	**02.7**	**04.9**	**07.7**

Alcı-Orhaniye (Miocene-Pliocene, vol.)																						
R 13	39.90372°	32.50336°	L.-M. Miocene		22	25 / 25	356.4	07.3	58.4	05.2	053.3	04.0							027.2	39.1	03.3	05.6	10.8
Tekke**	39.74768°	32.53028°	L.-M. Miocene		06	06 / 05	335.9		77.5	16.3	023.7	16.0							008.1	66.2	06.3	28.6	29.7
Mamak**	40.01553°	32.90514°	L.-M. Miocene		08	08 / 07	352.0	19.8	40.9	24.6	013.6	17.0							012.1	23.4	05.5	18.1	24.1
Bozdağ**	39.85689°	32.58413°	L.-M. Miocene		03	03 / 03	144.8	50.1	-66.9	21.8	041.4	19.4							018.1	-49.6	07.7	29.9	41.0
Mean (N)						**39 / 35**	**354.2**	**07.0**	**55.8**	**05.5**	**027.4**	**04.7**							**019.7**	**36.4**	**02.9**	**05.6**	**08.7**
Mean (N+R)						**14 / 18**	**346.5**	**14.7**	**54.0**	**12.3**	**014.4**	**10.8**							**011.8**	**34.5**	**04.2**	**12.1**	**15.6**
Northern Haymana (Miocene-Pliocene)																						
R 24	39.49088°	32.42698°	Pliocene		25	23 / 23	158.8	08.2	-60.7	05.2	048.2	04.4	167.5	05.9	-47.0	06.2	048.2	04.4	035.4	-28.2	03.4	05.2	11.4
R 27	39.63345°	32.19992°	Pliocene		17	17 / 17	349.2	07.5	61.2	04.7	082.5	04.0	327.7	05.7	50.3	05.4	082.5	04.0	055.0	31.0	03.9	04.9	13.8
R 31	39.66499°	32.16552°	Middle Miocene		34	20 / 20	350.2	04.9	50.7	04.6	085.3	03.6							062.1	31.4	03.6	04.2	12.4
R 32	39.57138°	31.99519°	Pliocene		32	28 / 28	001.5	07.8	56.3	06.0	032.5	04.9							020.1	36.9	03.2	06.2	10.0
Mean (N+R)						**88 / 88**	**351.0**	**04.0**	**57.4**	**03.0**	**039.7**	**02.4**	**347.9**	**03.8**	**51.7**	**03.4**	**036.1**	**02.6**	**023.6**	**32.3**	**02.0**	**03.2**	**04.9**
Southern Haymana (Miocene)																						
~~SF 2~~	38.63961°	32.85627°	Middle Miocene		20	18 / 12	No reliable result																
~~SF 5~~	38.89064°	32.33443°	Middle Miocene		15	13 / 05	No reliable result																
~~SF 6~~	38.98257°	32.33974°	Middle Miocene		16	11 / 11	No reliable result (Present day remagnetization)																
R 4	39.22803°	31.90884°	Middle Miocene		46	30 / 30	346.1	07.3	54.0	06.1	031.7	04.7	326.0	08.0	57.2	05.9	031.7	04.7	018.2	37.8	03.1	06.3	09.6
Southern Haymana (Miocene, vol.)																						
R 45	39.20876°	32.70327°	Middle Miocene		34	13 / 12	209.1	08.3	-23.7	14.3	029.1	08.2							029.4	-12.4	04.4	08.1	17.1
~~R 46~~	39.21776°	32.85851°	~~Miocene~~		~~24~~	~~24 / 24~~	~~005.9~~	~~07.8~~	~~54.3~~	~~06.5~~	~~031.9~~	~~05.3~~	~~002.6~~	~~04.3~~	~~-01.4~~	~~08.7~~	~~031.9~~	~~05.3~~	~~047.6~~	~~-00.7~~	~~03.4~~	~~04.3~~	~~11.1~~
Southern Haymana (Pliocene)																						
R 3	39.21949°	32.06600°	Pliocene		35	16 / 16	016.3	12.5	68.4	05.4	053.7	05.1							023.8	51.6	04.0	07.7	14.3
R 5	39.39786°	32.10578°	Pliocene		23	14 / 12	183.9	10.1	-28.6	16.2	018.2	10.0	179.6	10.7	-41.5	13.1	025.3	08.8	020.8	23.8	04.4	09.8	17.1
R 37	39.26698°	32.26085°	Pliocene		26	16 / 16	177.7	10.8	-39.1	14.0	014.6	10.0	190.7	12.0	-47.7	12.4	016.9	09.6	014.2	28.8	04.1	10.5	14.9
R 50	39.15034°	32.50766°	Pliocene		20	10 / 06	154.6	15.9	-44.1	18.1	020.8	15.1							023.1	25.9	05.9	14.2	26.5
R 51	39.17460°	32.39708°	Pliocene		20	24 / 24	184.3	09.0	-29.0	14.3	012.7	08.6							012.6	-15.5	03.4	08.7	11.1
~~SF 1~~	38.72170°	32.81770°	Pliocene		19	14 / 0	No reliable result																
~~SF 3~~	38.79057°	32.57749°	Pliocene		20	14 / 0	No reliable result																
SF 4	38.89749°	32.60258°	Pliocene		16	11 / 11	203.2	12.0	-42.0	14.6	022.3	09.9							018.3	-24.2	04.6	11.0	18.1
Mean (N)						**44 / 44**	**005.6**	**07.1**	**60.9**	**04.5**	**030.8**	**03.9**							**017.6**	**41.9**	**02.6**	**05.3**	**07.6**
Mean (R)						**54 / 50**	**183.2**	**05.4**	**-31.7**	**08.2**	**014.7**	**05.3**	**184.1**	**05.9**	**-37.1**	**08.0**	**014.3**	**05.5**	**014.3**	**-20.7**	**02.5**	**05.5**	**07.0**
Mean (N+R)						**98 / 96**	**004.0**	**04.9**	**45.3**	**04.9**	**012.2**	**04.3**	**004.6**	**05.0**	**48.8**	**05.0**	**013.5**	**04.1**	**011.9**	**29.7**	**01.9**	**04.4**	**04.6**

*Parametric bootstrap resampling from; *: Çinku et al., 2016; **: Piper et al., 2010.*

5.2 Tuz Gölü (TG)

Tuz Gölü Domain comprises the southwestern flank of the Kırşehir Block and straddles the Intra-Tauride Suture Zone. It is delimited by the Menderes-Tauride Block in the west. The sampled horizons range from Middle Miocene to Pliocene. Except for one disregarded site (R78), all other three sites produced statistically meaningful results. In addition, one site (TT8, Oligo.-Miocene in age) is added to the domain from literature (Çinku, 2017) and it was parametrically re-sampled and then combined with our results (Fig. 4). The Oligo-Miocene site (TT8, N=8) shows 327.0 ± 12.9°/60.5 ± 8.3°, declination/inclination values, which indicates approximately 33° counterclockwise (CCW) rotation of the locality. The remaining two Miocene to Pliocene sites show normal (R18, TT8) and reversed (R84) polarities, all of which indicate coherent CCW rotations. The combined result suggests that the Tuz Gölü domain underwent approximately ~15 ± 5° average CCW vertical-axis rotation since the Miocene (Fig. 4, Table 1). Considering the limited number of sites for each age, we cannot discriminate differential rotation from Miocene to Pliocene times. However, the reversal test of all three sites produced a positive result (Fig. 5), suggesting that no significant differential rotation took place within that age interval and main rotation took place by the end of Miocene - Pliocene.

5.3 Alcı-Orhaniye (AO)

This Alcı-Orhaniye Domain is located in the northwestern part of the study area, within the Pontide Block. From this domain, we sampled 10 sedimentary sites, of which 6 belong to Upper Miocene and 4 to Pliocene sequences. The sites display both normal and reversed polarities. Three sites were disregarded, since they produced no meaningful results, either because of lightning (S2), a recent remagnetization as indicated by too steep inclination after tilt correction (S3), or an anomalously large CCW rotation (S6) that does not fit with the adjacent sites. Since the domain has a sufficient number of reliable site results for different time intervals, the results are divided into two different time intervals, i.e. for the Miocene and Pliocene ages. The Miocene normal polarity sites indicate a well clustered VGP distribution (K = 30.4, A_{95} = 4.6) and mean ChRM direction of D = 329.2 ± 5.0° / I = 41.6 ± 6.2° after tilt correction (Table 1), which indicates approximately 30° CCW rotation. Furthermore, the reversed polarity sites (S5 and R30) present a very similar mean direction indicating mean rotation of ~24° CCW. The reversal test, however, is negative possibly because of shallow inclinations of the reversed sites. Nevertheless, they become significantly steeper after tilt correction. Combining the normal and reversed Miocene sedimentary sites shows mean direction of D = 332.4 ± 4.0° / I = 39.1 ± 5.2°. This indicates that the Alcı-Orhaniye Domain has rotated approximately 27° CCW since the Miocene. Furthermore, the remaining three Pliocene sites (S4, R28, R29) have normal magnetization directions, and they also produced similar rotations around 22° CCW (D = 337.7 ± 5.5°). Additionally, three volcanic localities from Piper et al. (2010) of Miocene (Tekke, Mamak) and-Pliocene (Bozdağ) age also indicate CCW rotation (Table 1). The mean of the combined analysis of volcanic sites of Piper et al. (2010) and our single basalt site (R13) indicate approximately 14° CCW rotation. However, the error in declination values is quite large (D = 346.5 ± 14.7°) implying that their rotation can be considered as conformable with the sedimentary sites. In conclusion, all these results indicate that mean of Pliocene sites are slightly lower than the Miocene sites implying that rotation started during the Late Miocene and continue during the Pliocene.

5.4 Northern Haymana (NHY)

The Haymana Basin is traversed by Yenimehmetli Fault (Fig. 1) strike-slip fault that compartmentalized the basin into two domains. Therefore, the northern and southern parts of the basin are analyzed separately. The Northern Haymana Domain is delimited in the northeast by the Hirfanlar Hacıbektaş Fault and in the south by the Yenimehmetli Fault (Fig. 1). In the west it is delimited by the İzmir-Ankara Suture. It comprises four paleomagnetic sites; one site (R31) from the Miocene and three sites (R24, R27) from the Pliocene. The Miocene site mean yields a ~10° CCW rotation with a small error (D = 350.2 ± 4.9°). The three Pliocene sites have both normal (R27 and R32) and reversed (R24) polarities. The combined Mio-Pliocene directions resulted in D = 347.9 ± 3.8°, which indicate approximately ~12° CCW mean rotation for the domain. (Table 1), contrary to the results obtained from the Pliocene localities in the Southern Haymana Domain (Fig. 4, Table 1), see below. The reversal test was applied to tilt corrected data, but it is found to be negative (Fig. 5).

5.5 Southern Haymana (SHY)

The Southern Haymana Domain is delimited in the NE by the Hirfanlar-Hacıbektaş Fault Zone, Yenimehmetli Fault in the NW and Intra-Tauride Suture in the west and Ankara-Erzincan Suture in the east. The domain comprises 12 sedimentary sites, 4 of which belongs to Middle Miocene and remaining 8 sites belong to Pliocene sequences (Table 1). In addition, two volcanic layers (R45 and R46, Miocene basalt lavas) were also sampled in the domain. Each volcanic site contains at least seven different lava layers. All of the Miocene sedimentary sites shows normal polarities. Three of them were disregarded for final analysis since they present scattered NRM directions in two sites (SF2 and SF5) and the site SF 6 seems to be remagnetized by the recent magnetic field, after deposition. The remaining site R 4 is located in the southwesternmost of the study area and shows a well-clustered distribution ((Fig. 4, Table 1) which gave a quit large mean rotation after tilt correction compared to in-situ rotation result. The site yielded D = 326.0± 8.0°/I = 57.2 ± 5.9° indicating an approximately 34° CCW rotation since the Miocene. The South Haymana Domain includes two volcanic sites, but site R46 shows nearly horizontal inclinations after tilt correction and is disregarded. The remaining site (R45) indicate reversed polarity with mean directions of D = 209.1 ± 8.3°/I = -23.7 ± 14.3°. This indicates approximately 30° CW rotation, opposite to the nearby sedimentary site (R4).

For the Pliocene rotation history of the domain, sampled 8 sites are sampled. They show both normal and reversed polarities. Two sites (SF1, SF3) were disregarded due to the scattered nature of the NRM directions (Fig. 4). Two normal polarity sites (R3, R32) have a mean (N= 44) showing no significant rotation (D = 5.6±7.1°). The remaining 5 sites have reverse polarity, and similarly, they also show no significant rotation (D = 4.1±5.9°) after tilt correction. This is almost in line with the results from the Pliocene Polatlı lavas (Piper et al., 2010) (Table 1) which show a small CW rotation. As a conclusion, the southern Haymana locality indicates, on average, no significant rotation (D = 4.0 ± 4.9°) since the Pliocene. The only successful Middle Miocene site (R4) is far from representing the Miocene rotation history of the domain. Interestingly, it contradicts with the result of the single Miocene volcanic site (R45), which is located at the outer rim of the domain.

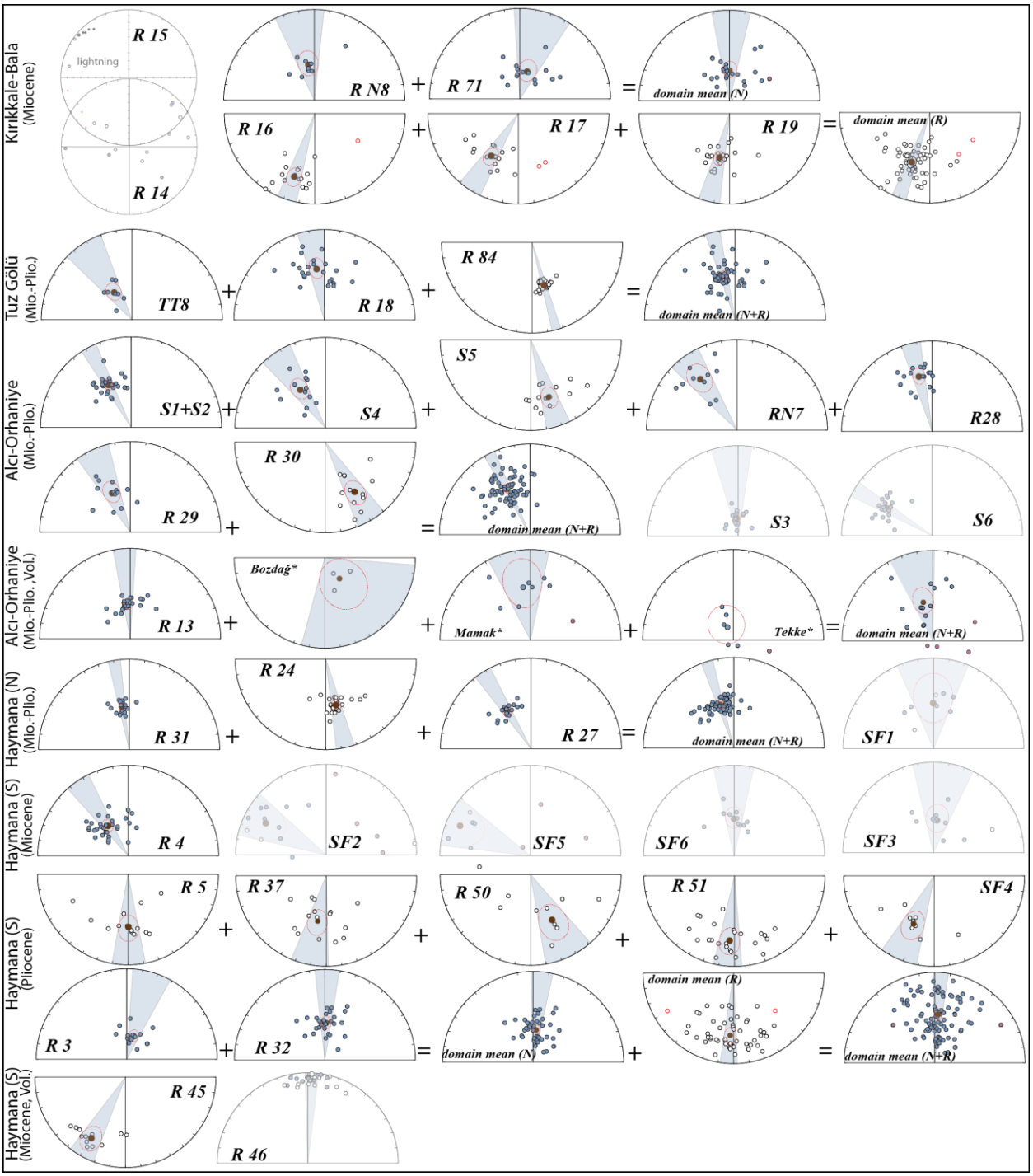

Figure 4. Equal area projections of ChRM directions for each domain and their means with associated error ellipses (ΔDx, ΔIx) according to Deenen et al. (2011), after tectonic correction (TC). Rejected directions (after 45^{o} cutoff) are displayed in red, and normal (reverse) directions are shown as solid (open) circles. All directions have been converted to normal polarity to average for each domain results (see also Table 1, 2).

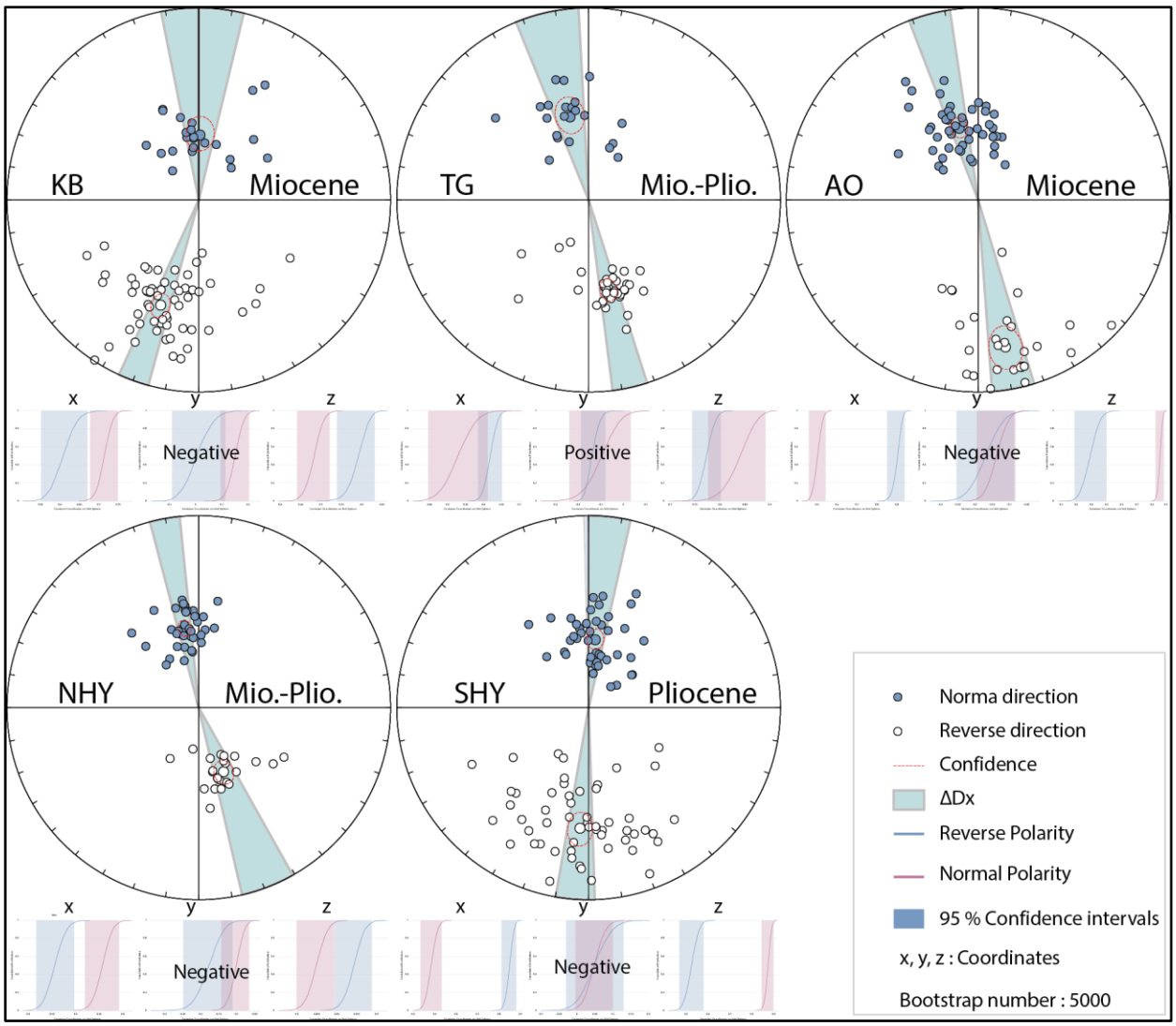

Figure 5. Equal area projection of the ChRM directions for each domain. Closed (open) symbols indicate projection on lower (upper) hemisphere. Red dashed circles denote the mean directions and their cone of confidence (α95). Reversals test results are calculated by the coordinate bootstrap method of Tauxe (2010).

6 Evaluation of published data

Several paleomagnetic results have been published in the region. Most of these studies are based on magmatic rocks except for a few sedimentary studies. The studies on the magmatic rocks are mainly concentrated on two large Neogene volcanic provinces, namely Cappadocian and Galatean Volcanic provinces, and the granitic rocks within the Kırşehir Block. The studies on the sedimentary rocks are concentrated mainly on the Çankırı Basin. We have evaluated each rock type and tectonic domain in detail below.

6.1 Cappadocian Volcanic Province (CVP)

In the south-easternmost part of the study area, the Cappadocian Volcanic Province (CVP) consists of Neogene to Quaternary ignimbrites, basalt flows covered by epiclastic

lacustrine sequences (Aydar et al., 2013). Miocene to Quaternary paleomagnetic results from the CVP belongs to three different studies (Gürsoy et al., 1998; Özçep, 2010; Platzman et al., 1998). These studies include various lava levels from three different sites spanning from Middle Miocene to Quaternary. They produced very consistent CCW results. The integrated results from all sites indicate that the region has been rotated about 12 ± 6° counterclockwise since the middle Miocene to Quaternary (Fig.6, Table 2).

6.2 Galatean Volcanic Province (GVP)

The Galatean Volcanic Province is located at the northwest of the study area and comprises Neogene volcanic rocks (Tankut et al., 1999; Toprak, 1998, 1994; Wilson et al., 1997). Gürsoy et al. (1999), Çinku and Orbay (2010) have studied the region and they reported results from five different localities belonging to Neogene rocks (Figures 1&6). The locality (AYS) comprises two different sites and shows low inclination and large declination results (D=247.0±3.3°/I=7.2±6.5°). Therefore, we rejected these sites for further analysis from our database (Table 2). The BYP locality includes 3 distinct lava levels and their combined results produced D:65.6°, I=63.6°, implying very large (~65°) CW rotation of the area since Miocene. The KBR locality, contains 9 lava levels and 2 andesitic suits, combined results of which indicate ~18.5° CW rotation (Table 2). Unlike other localities in the region, site ST has reversed polarity but it also indicates a CW rotation of 31° (Table 2). The KCH locality has 8 different lava levels and mean rotation result indicate a very significant CCW rotation amount (~36.5°) unlike other sites in the GVP. Combined analysis of only CW sites indicate 27° CW rotation while combination of all four sites indicate ~20.0° CW rotation in the GVP during Upper Miocene-Pliocene (Table 2, Fig. 6).

6.3 Çankırı Basin (ÇB)

The Çankırı Basin is located at northeasternmost part of the study area, at the northern tip of Kırşehir Block, where Ankara-Erzincan Suture Zone makes an omega-shaped northwards convex bend. The area comprises 11 sedimentary sites ranging from Middle to Upper Miocene belonging to three different studies (Çinku et al., 2016; Hisarlı et al., 2016; Kaymakcı et al., 2003a; Lucifora et al., 2013). According to Kaymakcı et al. (2003a), the basin underwent counter-clockwise and clockwise rotations in its western and eastern margins respectively, due to indentation of the Kırşehir Block. We have parametrically resampled the results of these studies and found out that 5 of the 12 sites show reverse polarity and their mean rotation amount is changing from ~27° CCW to ~22° CW (Table 2). Similarly, the remaining 7 sites show both CW (max=25.6°) and CCW (max=30.8°) rotations. Very large variations in rotation amounts and sense in such a small region indicate that the basin underwent internal deformation during the Neogene. The results show both normal and reversed polarity data. Therefore, no reversal test is applied to the data and they are not used for further analysis.

6.4 Kırşehir Block

The Kırşehir Block is one of the largest metamorphic terranes in Central Turkey and is bordered by Ankara-Erzincan Suture Zone in the north, the Tuz Gölü Fault Zone in the west, and Intra-Taruide Suture Zone in the south and east. Lefebvre et al. (2013) studied the plutonic rocks of the block and proposed 3 different rigid fault blocks that deformed independently during the Late Cretaceous to Tertiary. These three fault blocks of the Kırşehir Block are separated by approximately NW-SE striking fault zones developed possibly by the end of Cretaceous as

normal faults providing accommodation space for Çiçekdağı and Ayhanlar basins (Fig. 1). The fault blocks of the Kırşehir Block, from south to north include Ağaçören-Avanos Block (AAB). It is delimited in the north by the Haymana-Hirfanlar Fault Zone. Kırşehir-Kırıkkale Block (KKB) constitutes the middle part of the Kırşehir Block and it is delimited in the north by the Haymana-Hirfanlar Fault Zone while Delice-Kozaklı FZ delimits it in the north. The northern block of the Kırşehir Block is the Akdağ-Yozgat Block (AYB). It is separated from the other blocks of the Kırşehir Block by the Delice-kozaklı FZ in the south. Lefebvre et al. (2013) proposed 35° CCW for the AAB, 6° CCW rotations for the KKB and 15° for the AYB (Table 2, Fig. 6).

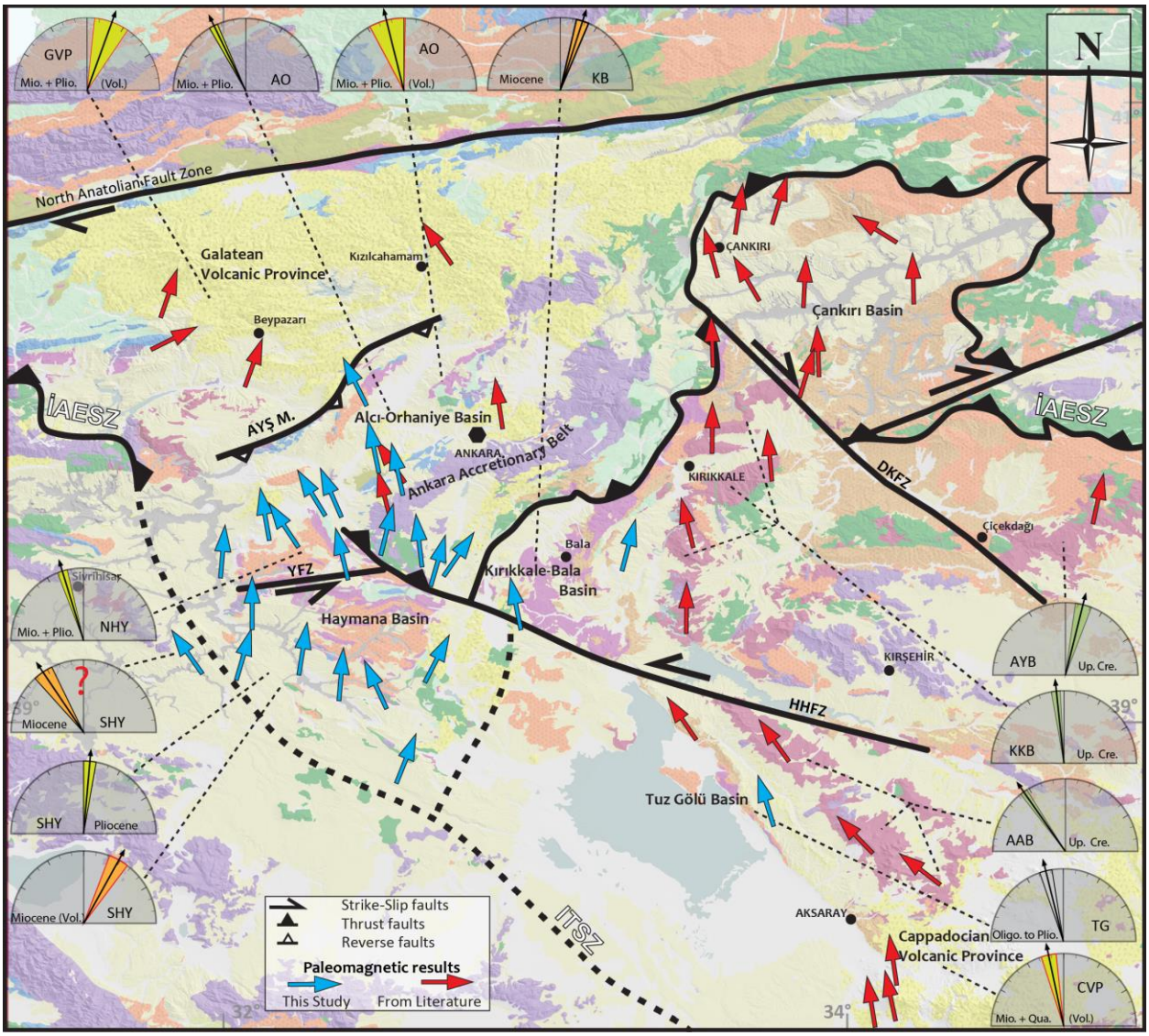

Figure 6. Arrows show individual site results both this (blue) and literature (red). Domains and associated vertical axis rotations are denoted as arrows on equal area projection with their 95% error envelope (ΔDx).

Table 2. Table showing all published Neogene paleomagnetic results from the Central Anatolia. See Table 1 for explanations of the symbols and abbreviations.

Site/Locality	*Lat. (N°)*	*Long. (E°)*	*Age*	*ChRM directions (tilt adjusted)*										
				Dec	*ΔD*	*Inc*	*ΔI*	*k*	*a95*	*K*	*λ*	$A95_{min}$	*A95*	$A95_{max}$
Cappadocian Volcanic Province														
[1]HSN	38.01575°	34.07733°	M. Miocene	350.1	19.1	57.6	13.8	031.8	10.9	017.4	38.3	05.5	14.9	024.1
[2]AKS	38.16052°	34.07070°	Pliocene	350.5	11.9	57.6	08.7	036.6	08.1	027.8	38.2	04.8	09.3	019.2
[3]HD&MD	38.11583°	34.11515°	Plio-Quater.	347.6	12.4	41.4	15.2	032.3	12.0	036.0	23.8	05.9	11.3	026.5
All NCVP				348.4	06.1	52.9	05.3	031.6	04.5	025.4	33.5	03.0	05.1	009.1
Galatean Volcanic Province														
[4]~~AYS~~	40.03200°	32.33500°	U. Mio.-Plio.	~~246.2~~	~~18.1~~	~~08.2~~	~~35.6~~	~~050.6~~	~~35.8~~	~~193.3~~	~~04.1~~	~~09.1~~	~~18.1~~	~~053.0~~
[4]BYP	40.21100°	31.93000°	U. Mio.-Plio.	065.6		63.6	45.9	045.6	37.9	020.9	45.2	09.1	57.6	053.0
[4]KBR	40.23000°	31.92661°	U. Mio.-Plio.	018.6	14.5	56.8	10.9	032.6	09.2	021.2	37.4	05.0	11.5	020.5
[4]KCH	40.5519°	32.69512°	U. Mio.-Plio.	323.4	36.9	54.2	30.0	007.7	25.7	006.1	34.7	05.9	29.6	026.5
[5]ST	40.14178°	32.11717°	U. Mio.-Plio.	211.1	34.7	-55.6	26.8	040.7	19.6	021.4	-36.1	07.7	27.3	041.0
CW sites only				026.8	13.3	58.4	09.4	028.2	07.6	015.8	39.1	04.2	10.3	015.6
All SGVP				**020.1**	**13.7**	**57.7**	**10.0**	**018.2**	**08.6**	**012.0**	**38.4**	**03.9**	**10.7**	**013.8**
Çankırı Basin														
[6]HAL1	40.15949°	33.89265°	M. Miocene	197.3	15.4	-25.9	25.6	017.8	18.7	027.3	-13.6	06.3	14.9	029.7
[6]UR	40.21122°	33.93793°	U. Miocene	352.3	16.9	47.5	17.5	012.6	19.6	021.5	28.6	05.9	14.8	026.5
[6]KUC	40.16605°	34.02077°	M. Miocene	183.0	09.0	-57.7	06.5	126.6	05.6	074.1	-38.4	05.5	07.1	024.1
[7]KS22	40.23618°	33.58103°	M. Miocene	358.1	18.7	66.1	09.2	047.5	08.1	021.3	48.5	05.2	12.3	022.1
[8]BO01			U. Miocene	329.3	05.4	39.7	06.9	032.9	06.1	048.8	22.5	03.8	05.0	013.3
[8]BO02_r			U. Miocene	152.9	13.6	-51.5	12.4	029.3	10.4	024.2	-32.1	05.2	11.5	022.1
[8]BO03			U. Miocene	020.9	15.3	63.0	08.8	033.1	07.3	015.5	44.5	04.3	10.9	016.3
[8]BO04			U. Miocene	006.2	06.4	45.7	07.0	34.5	05.6	033.7	27.1	03.6	05.7	012.4
[8]SU01			U. Miocene	205.4	07.3	-45.4	08.0	068.1	06.8	074.1	-26.9	05.2	06.5	022.1
[8]SU02			U. Miocene	189.2	06.9	-44.7	07.8	063.9	06.5	069.9	-26.3	05.0	06.2	020.5
[8]TU01			U. Miocene	019.9	06.4	55.1	05.1	048.5	04.4	035.0	35.6	03.4	05.2	011.4
Mean (N)				**001.6**	**05.1**	**53.3**	**04.4**	**018.8**	**03.6**	**014.0**	**33.8**	**02.0**	**04.3**	**005.0**
Mean (R)				**187.8**	**06.5**	**-47.4**	**06.8**	**019.7**	**05.4**	**018.1**	**-28.5**	**02.8**	**05.7**	**008.4**
Mean (N+R)				**003.6**	**04.1**	**51.5**	**03.7**	**018.7**	**03.0**	**014.8**	**32.2**	**01.8**	**03.4**	**004.0**
Kırşehir Block														
[9]AYB			U. Cretace.	014.5	06.2	54.4	05.1			012.9	34.9	03.2	05.1	005.9
[9]KKB			U. Cretace.	353.9	03.6	57.7	02.6			014.0	38.3	02.1	02.8	002.9
[9]AAB			U. Cretace.	324.8	03.2	51.3	03.0			014.8	32.0	02.1	02.7	003.0

Parametric bootstrap resampling from; 1: Gürsoy et al., 1998; 2: Platzman et al., 1998; 3: Özçep, 2010; 4: Gürsoy et al., 1999; 5: Çinku and Orbay, 2010; 6: Kaymakcı et al., 2003; 7: Çinku et al., 2016, 8: Lucifora et al., 2013. Site results taken from, 9: Lefebvre et al., 2013.

7 Discussion

7.1 Neogene Block rotations in Central Anatolia

The new paleomagnetic results from more than 900 specimens collected from 39 new sites are documented here, as well as existing literature data reported from 27 sites, which we assessed and parametrically resampled in order to homogenize and unify them with our data. They are altogether used to developed rotational evolutionary scenarios of central Anatolia and to reconstruct the Neogene geometry of Neotethyan sutures in Turkey.

All paleomagnetic results covering Miocene to Quaternary sedimentary and volcanic rocks are considered to be of primary origin demonstrated by reversal tests (Tauxe, 2010) and other paleomagnetic criteria (e.g. rock magnetic analysis, PSV check). Of the 39 analyzed sites, only 9 of them (~25%) were rejected due to scattered ChRM directions, lightening effect, and inconsistent demagnetization behaviours marked in Table 1.

The remaining 75% of the data passes all the tests, and we regard them as reliable and interpretable. The reliable data are separated into subgroups based on the tectonic domain they belong. Eighth domains are separated in this study. These are Kırıkkale-Bala Domain (KB), Tuz Gölü Domain, (TG), Alcı-Orhaniye Domain (AO), Northern Haymana Domain (NHY), Southern Haymana Domain (SHY), Cappadocian Volcanic Province (CVP), Galatian Volcanic Province (GVP), and Çankırı Basin (Table 1 and 2, Fig. 6 and 7). The boundaries of these domains are defined by a major structure such as suture zones or a well-developed fault zones (Gülyüz et al., 2019; Lefebvre et al., 2013; Özsayın and Dirik, 2007).

The Kırıkkale-Bala Domain partly belongs to Kırşehir-Kırıkkale Block (KKB) of Lefebvre et al. (2013) while Tuz Gölü Domain lies within the Ağaçören-Avanos Block (AAB) (Lefebvre et al., 2013).

According to our rotation results, two of our localities (R18 and R71, Fig. 1) located within the KKB of Lefebvre et al. (2013) indicate CW and CCW rotation. It is possible that these two localities are caught within the Hirfanlar-Hacıbektaş Fault Zone (Lefebvre et al., 2013) and produced opposite rotations (Fig. 6). The combined results from Kırıkkale-Bala Domain indicate a mean CW rotation of ~18° by the Late Miocene (Table 1), contrary to the approximately ~6° CCW (negligible) rotation obtained from the Late Cretaceous-Paleogene intrusive suits of the KKB (Lefebvre et al., 2013).

According to various publications, the Çankırı Domain shows various normal and reversed directions indicating CW as well as a few CCW rotations. The combined analysis of normal polarities indicate no net rotations (D:1.6±5.1°) while reversed polarity sites indicate approximately ~8° CW rotations. Combining all sites indicates approximately no net rotation in the Çankırı Domain. (Table 2, Fig. 6). The Çankırı Domain is associated with the Akdağ-Yozgat Block (AYB) of Lefebvre et al. (2013), and they reported that the Upper Cretaceous intrusive suits within the block rotated ~15° CW. Having no net rotations in the Çankırı Domain indicate that the rotation of AYB took place prior to late Miocene.

Among the four sites from the Tuz Gölü Domain, only three sites produced reliable results. Combined analysis of these sites indicates that approximately ~14° CCW rotation of the domain. The Tuz Gölü Domain is located within the Ağaçören-Avanos Block of (Lefebvre et al., 2013) late Cretaceous Intrusive suits of which rotated approximately ~35° in CCW sense. Our results indicate a similar sense of rotation, whereas they are almost half the rotation of the AAB. Similarly, paleomagnetic studies carried out in the Cappadocian Volcanic Province (e.g. Gürsoy et al., 1998; Özçep, 2010; Platzman et al., 1998), which is located within the AAB also shows

approximately ~ 12° CCW rotation since the middle Miocene. All these results indicate that almost half of the CCW rotations of the AAB took place by the Miocene and onwards and the remaining -20° CCW rotation took place prior to Miocene.

The results of Alcı-Orhaniye Domain indicate approximately ~27° CCW rotations for the upper Miocene and ~22 CCW rotations for the Pliocene sequences. This relationship indicates that the rotations in the domain started in the Late Miocene and only about ~5° CCW rotation took place. However, the main rotation took place by the Pliocene.

The Northern Haymana Domain rotated approximately ~12 in CCW sense while rotation amounts in the Southern Haymana Domain range from ~34° during the Miocene, though only one site produced reliable results, to almost no net rotation (4.6 ± 5°) during the Pliocene.

The results from Galatean Volcanic Province indicate approximately ~20° CW rotations (Çinku and Orbay, 2010; H Gürsoy et al., 1999) contrary to the nearby Alcı-Orhaniye and Haymana domains (Table 2, Fig. 6).

7.2 Temporal Relationships

Our paleomagnetic data combined with parametrically bootstrapped literature data show that rotational deformation in Central Anatolia is a continuous process post late Cretaceous times and various rotation amounts and senses took place in different domains of the region. There are significant variations both in the senses, and the amounts of the vertical-axis block rotations since the early Miocene and in some domains rotations took place during the Early Miocene and lasted until Pliocene while some took place after Pliocene (Fig. 7).

For the Kırıkkale-Bala Domain, there is only data for the Upper Miocene to Pliocene time interval because available age data do not allow better age resolution for the sampled horizons in the domain. However, TT8 site of Tuzgölü Domain (Çinku et al., 2016) indicate 33° CCW rotation of the Oligo-Miocene sequences while our Miocene and Pliocene sedimentary sites indicate approximately ~12° CCW rotations. This relationship indicates that CCW rotation started before the Late Miocene and continued afterwards. Rotation amount of the TT8 site is almost equal to the rotation amount of AAB of Lefebvre et al. (2013) implying that the rotation of the Block took place by the Miocene and continued onwards.

Rotation amounts in the Alcı-Orhaniye Domain are almost the same, considering the error margins, for Miocene (D:332.4±4) and Pliocene (D:337.7±5.5) sequences. This relationship indicates that the main rotations in the domain took place after the Late Miocene.

The Northern Haymana Domain comprises three Pliocene and one middle Miocene sites. The results of all sites are almost equal to each other, implying that rotations took place post-Miocene times. Combined analysis of all sites indicates approximately ~12° CCW rotation for the Northern Haymana Domain during Pliocene.

Only one Miocene site produced reliable result from the Southern Haymana Domain which indicates an approximately ~34° CCW rotation, while Pliocene sites indicate no significant rotation, implying that rotations took place prior to Pliocene.

In conclusion, obtained rotation amounts, senses, and their timing indicate that rotational deformation of the Central Anatolia is diachronous and it cannot be constrained to a specific single time interval.

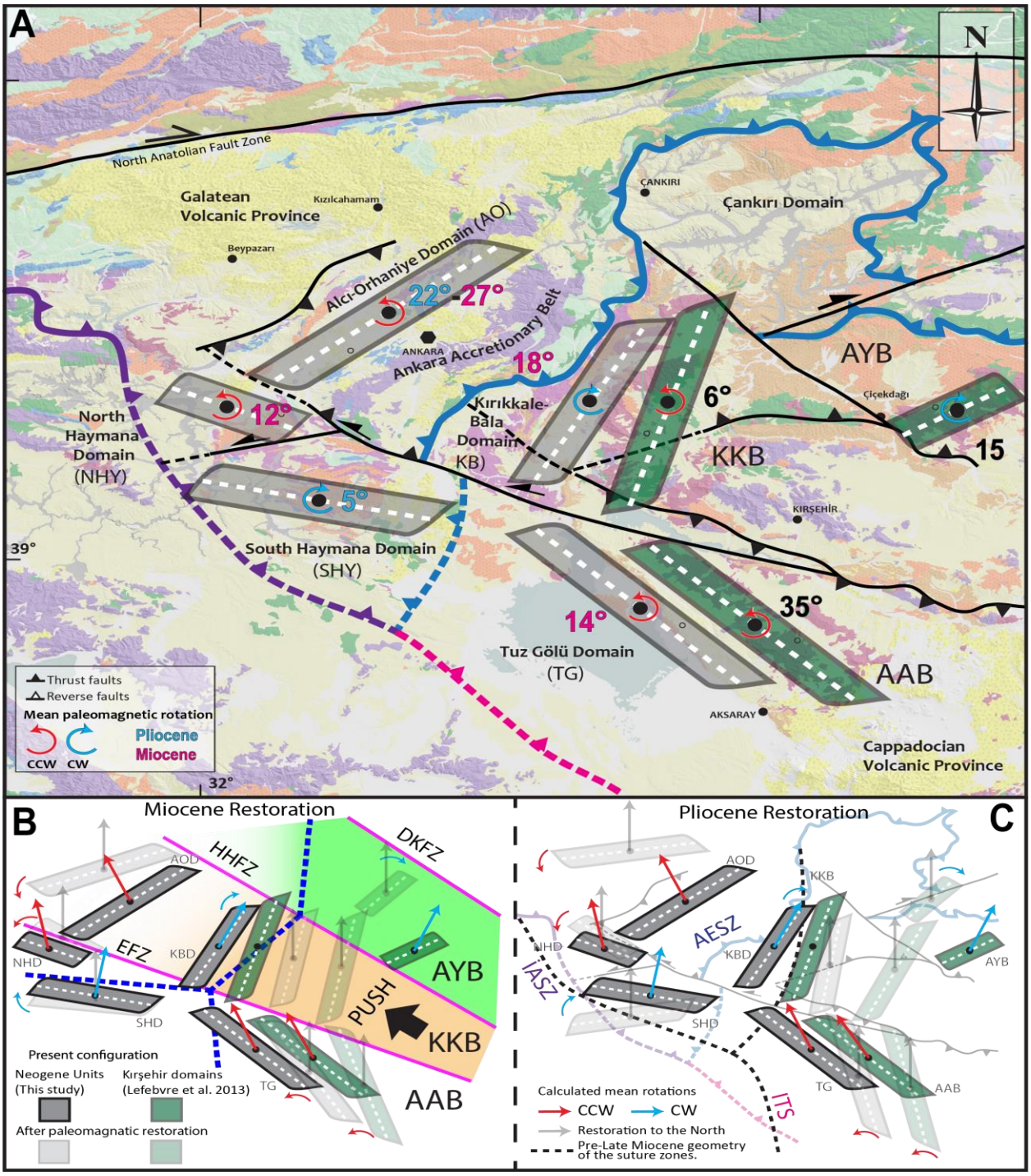

Figure 7. Kinematic restorations of Central Anatolia and Neotethyan Suture in central Anatolia. a) Rotation amounts and representative blocks for each domain with before and after restoration. Restoration scenario for b) Miocene and c) Pliocene time intervals with major faults and fault blocks that controlled the deformation in the region. Highlighted gray domains are present-day configuration and three green blocks are after Lefebvre et al. (2013). Faint blocks are configurations before rotation took place. Red arrows indicate counter-clockwise rotation (CCW). Blue arrows show clockwise rotation (CW). Faint black arrows represent the present-day geographic north direction.

7.3 Orocline Test

In order to test the validity of our model we have applied an orocline test (Pastor-Galán et al., 2017) between Tuz Gölü and Kırıkkale-Bala domains (Fig. 8). A bootstrapped total least squared orocline test was applied to reveal interlineation between the paleomagnetic vertical-axis block rotation amounts and bedding attitudes. To perform the test, seven paleomagnetic results, local bedding strikes from this study and regional fold axes trends obtained from geological maps of General Directorate of Mineral Research and Exploration (MTA) (Işıker, 2002) are used. According to the the applied bootstrapped total least squared orocline test, the slope of the regression line of m = 0.674 ± 0.16; between m = 1 (100% positive) and m = 0 (100% negative) (Fig. 8). The results with their error margins indicate that the orocline geometry was acquired in the Miocene-Pliocene time interval (~50-85%) and the remaining (~15-50%) deformation corresponds to post-Pliocene activity in the region.

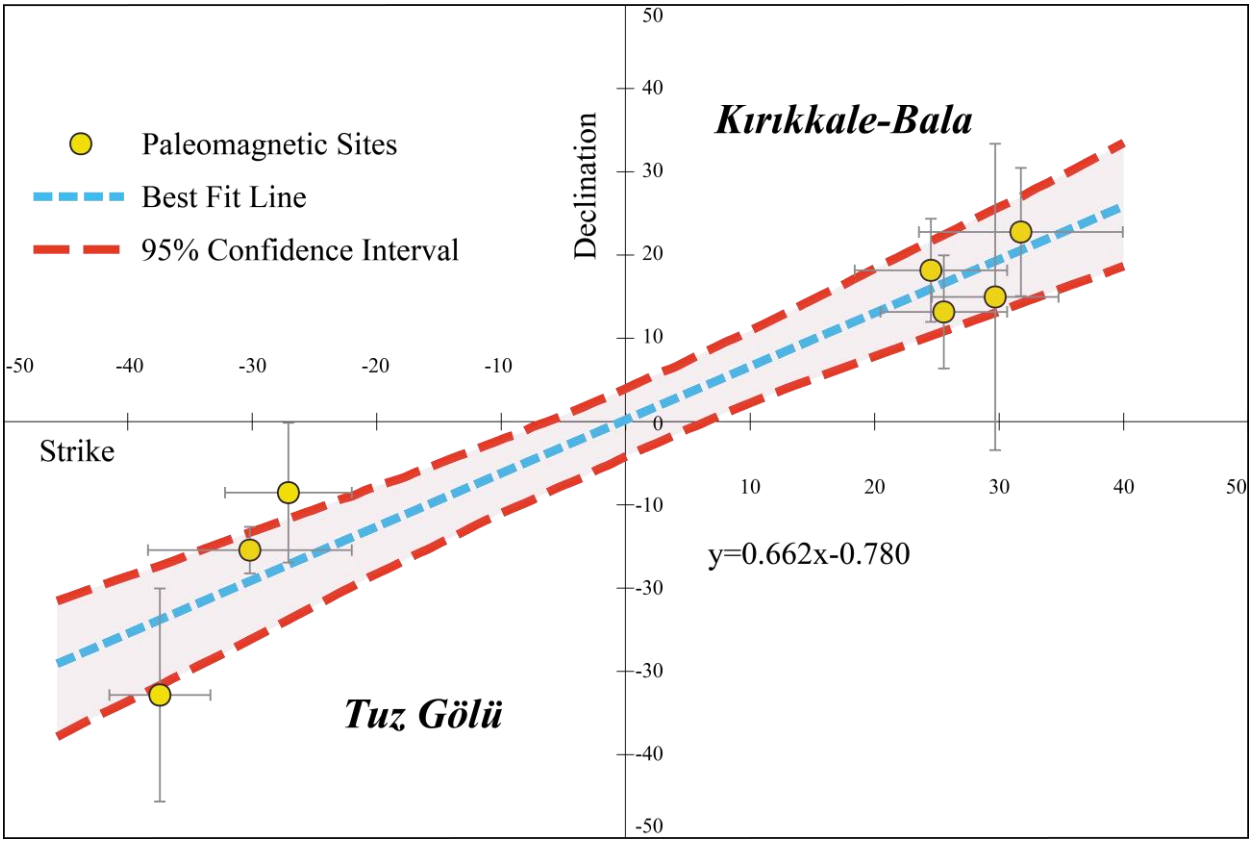

Figure 8. Orocline test based on paleomagnetic declination deviations for seven sites (in tectonic coordinates) relative to strike of the orocline.

7.4 Regional Implications and Kinematic Restorations

The main actors of the continental collision in the Central Anatolia include Kırşehir, Pontide, and Menderes-Tauride blocks. Various scenarios related to collision and further convergence of the region have been proposed in the literature. These scenarios can be classified into two groups; 1) Collision of Kırşehir Block as a rigid indenter into the Pontides along the İzmir-Ankara-Erzincan Suture Zone (Çinku et al., 2016, 2011; Kaymakcı et al., 2003a; Meijers et al., 2010), 2) collision of non-rigid magmatic arc model (Lefebvre et al., 2013).

Among these, the rigid Kırşehir Block models generally emphasize how and when the subduction and collision occurred in Central Anatolia and considered that the Pontides (Çinku et al., 2011; Kaymakcı et al., 2003a; Meijers et al., 2010) and Taurides (Çinku et al., 2016) deformed and curved around the rigid Kırşehir Block. The nonrigid Kırşehir model of Lefebvre et al. (2013) nicely illustrated how the Kırşehir Block was segmented and deformed during N-S shortening. Still, it fails to explain the timing of deformation and rotation of each block.

One of the main outcomes of this study is documentation of the diachronous nature of the rotational deformation in Central Anatolia and providing temporal and spatial constraints on the matter. Clearly, a uniform rotational history model with consistent counter-clockwise rotations for Central Anatolia since the Late Miocene (Çinku et al., 2016; Kissel et al., 2003; Koçbulut et al., 2013; Piper et al., 2010) is not a valid simplification, since the region was subdivided into smaller tectonic domains that have undergone variable rotation amounts and senses since the Miocene.

The obtained results are used to restore the geometry of the central Anatolia and the Neotethyan Suture Zones. As seen in Figure 7, the İzmir-Ankara Suture Zone (İASZ) becomes relatively E-W oriented compared to its present configuration, while the Intra-Tauride and Ankara-Erzincan suture zones become N-S oriented, although the change in the geometry of the suture zones is very small. However, they indicate the activity and timing of the block bounding faults. The results show that Delice-Kozaklı (DKFZ), Hirfanlar-Hacıbektaş and Eskişehir fault zones (HHFZ) were active during the Pliocene and possibly still active until recently, while the Yenimehmetli Fault was deactivated by the Pliocene. The deformation of the Kırıkkale-Bala and Alcı-Orhaniye domains seems to be due to westwards push of the Kırşehir-Kırıkkale Block (Fig. 7b); a V-shaped block tends to be moving in an NW direction while it is being squeezed in an N-S direction (Lefebvre et al., 2013).

8 Conclusions

Paleomagnetic results (this study and literature data) obtained through comprehensive sampling and analysis show evidence for a significant amount of rotations in Central Anatolia since Miocene. The main findings of this study are summarized as follows:

In addition to the previously published three separate fault blocks of the Kırşehir Block, five new tectonically distinctive domains are determined in this study. 1) Late Miocene strata in the Kırıkkale-Bala Domain rotated ~14° CW by the Late Miocene, 2) the late Miocene strata in the Tuz Gölü Domain rotated ~15° CCW by the Miocene, 3) Late Miocene sequences rotated approximately ~27° CCW in the Alcı-Orhaniye Domain while Pliocene sequences rotated approximately ~22 CCW indicating that the main CCW rotation phase took place after the Miocene in this domain, (4) Late-Miocene to Pliocene sequences in the Northern Haymana Domain rotated ~12° CCW, and (5) only one site produced reliable results from the Miocene sequences in the Southern Haymana basin, and Pliocene sequences underwent no significant rotation.

The geometry of the Neotethyan suture zone in the region prior to the late Miocene is restored, and it is found that the orientations of the Intra-Tauride and Ankara-Erzincan suture zones become almost N-S.

Acknowledgments

This study is part of PhD theses of Murat Özkaptan. Fieldwork has been partly supported by YÖK Grant of the Turkish Government. We used some paleomagnetic data from litreture and available through Gürsoy et al., 1998, 1999; Platzman et al., 1998; Özçep, 2010; Piper et al.,

2010; Çinku and Orbay, 2010; Kaymakcı et al., 2003; Çinku et al., 2016, Lucifora et al., 2013 and Lefebvre et al., 2013.

References

Advokaat, E.L., van Hinsbergen, D.J.J., Kaymakcı, N., Vissers, R.L.M., Hendriks, B.W.H., 2014. Late Cretaceous extension and Paleogene rotation-related contraction in Central Anatolia recorded in the Ayhan-Büyükkışla basin. Int. Geol. Rev. 56, 1813–1836.

Armijo, R., Meyer, B., Hubert, A., Barka, A., 1999. Westward propagation of the North Anatolian fault into the northern Aegean: Timing and kinematics. Geology 27, 267–270.

Aydar, E., Cubukcu, H.E., Erdal, Ş.E.N., Lütfiye, A., 2013. Central Anatolian Plateau, Turkey: incision and paleoaltimetry recorded from volcanic rocks. Turkish J. Earth Sci. 22, 739–746.

Burke, K., Şengör, A.M.C., 1986. Tectonic escape in the evolution of the continental crust. Reflect. Seismol. Cont. crust 14, 41–53.

Butler, R.F., 1992. Paleomagnetism: Magnetic Domains to Geologic Terranes. Blackwell Scientific Publications, Boston.

Çemen, I., Göncüoğlu, M.C., Dirik, K., 1999. Structural evolution of the Tuzgölü basin in Central Anatolia, Turkey. J. Geol. 107, 693–706.

Çinku, M.C., 2017. Paleomagnetic results from Northeast Anatolia: remagnetization in Late Cretaceous sandstones and tectonic rotation at the Eastern extension of the Izmir–Ankara–Erzincan suture zone. Acta Geophys. https://doi.org/10.1007/s11600-017-0097-7

Çinku, M.C., Hisarli, M., Hirt, A.M., Heller, F., Ustaömer, T., Kaya, N., Öksüm, E., Orbay, N., 2016. Evidence of Late Cretaceous oroclinal bending in north-central Anatolia: palaeomagnetic results from Mesozoic and Cenozoic rocks along the İzmir–Ankara–Erzincan Suture Zone. Geol. Soc. London, Spec. Publ. 425, 189 LP – 212.

Çinku, M.C., Hisarlı, Z.M., Heller, F., Orbay, N., Ustaömer, T., 2011. Middle Eocene paleomagnetic data from the eastern Sakarya Zone and the central Pontides: Implications for the tectonic evolution of north central Anatolia. Tectonics 30.

Çinku, M.C., Orbay, N., 2010. The origin of Neogene tectonic rotations in the Galatean volcanic massif, central Anatolia. Int. J. Earth Sci. https://doi.org/10.1007/s00531-008-0390-4

Dankers, P.H.M., 1978. Magnetic properties of dispersed natural iron-oxides of known grain size. Rijksuniversiteit te Utrecht.

Deenen, M.H.L., Langereis, C.G., van Hinsbergen, D.J.J., Biggin, A.J., 2011. Geomagnetic secular variation and the statistics of palaeomagnetic directions. Geophys. J. Int. 186, 509–520. https://doi.org/10.1111/j.1365-246X.2011.05050.x

Di Giuseppe, P., Agostini, S., Manetti, P., Savaşçın, M.Y., Conticelli, S., 2018. Sub-lithospheric origin of Na-alkaline and calc-alkaline magmas in a post-collisional tectonic regime: Sr-Nd-Pb isotopes in recent monogenetic volcanism of Cappadocia, Central Turkey. Lithos 316, 304–322.

Fisher, R.A., 1953. Dispersion on a sphere. Proc. R. Soc. London A217, 295–305.

Flerit, F., Armijo, R., King, G., Meyer, B., 2004. The mechanical interaction between the propagating North Anatolian Fault and the back-arc extension in the Aegean. Earth Planet. Sci. Lett. 224, 347–362.

Görür, N., Oktay, F.Y., Seymen, İ., Şengör, A.M.C., 1984. Palaeotectonic evolution of the Tuzgölü basin complex, Central Turkey: sedimentary record of a Neo-Tethyan closure. Geol. Soc. London, Spec. Publ. 17, 467–482.

https://doi.org/10.1144/GSL.SP.1984.017.01.34
Gülyüz, E., Durak, H., Özkaptan, M., Krijgsman, W., 2020. Paleomagnetic constraints on the early Miocene closure of the southern Neo-Tethys (Van region; East Anatolia): Inferences for the timing of Eurasia-Arabia collision. Glob. Planet. Change 185, 103089.
Gülyüz, E., Kaymakci, N., Meijers, M.J.M., Van Hinsbergen, D.J.J., Lefebvre, C., Vissers, R.L.M., Hendriks, B.W.H., Peynircioğlu, A.A., 2013. Late Eocene evolution of the Çiçekdağı Basin (central Turkey): Syn-sedimentary compression during microcontinent–continent collision in central Anatolia. Tectonophysics 602, 286–299.
Gülyüz, E., Özkaptan, M., Kaymakci, N., Persano, C., Stuart, F.M., 2019. Kinematic and thermal evolution of the Haymana Basin, a fore-arc to foreland basin in Central Anatolia (Turkey). Tectonophysics. https://doi.org/10.1016/j.tecto.2019.06.020
Gürsoy, H., Piper, J.D.A., Tatar, O., 2003. Neotectonic deformation in the western sector of tectonic escape in Anatolia: Palaeomagnetic study of the Afyon region, central Turkey. Tectonophysics 374, 57–79. https://doi.org/10.1016/S0040-1951(03)00346-9
Gürsoy, Halil, Piper, J.D.A., Tatar, O., 1999. Palaeomagnetic study of the Galatean Volcanic Province, north-central Turkey: Neogene deformation at the northern border of the Anatolian Block. Geol. J. 34, 7–23. https://doi.org/10.1002/(SICI)1099-1034(199901/06)34:1/2<7::AID-GJ812>3.0.CO;2-0
Gürsoy, H, Piper, J.D.A., Tatar, O., 1999. Palaeomagnetic study of the Galatean Volcanic Province, north-central Turkey: Neogene deformation at the northern border of the Anatolian Block. Geol. J. 34, 7–23.
Gürsoy, H., Piper, J.D.A., Tatar, O., Mesci, L., 1998. Palaeomagnetic study of the Karaman and Karapinar volcanic complexes, central Turkey: Neotectonic rotation in the south-central sector of the Anatolian Block. Tectonophysics 299, 191–211. https://doi.org/10.1016/S0040-1951(98)00205-4
Gürsoy, H., Tatar, O., Piper, J.D.A., Koçbulut, F., Akpinar, Z., Huang, B., Roberts, A.P., Mesci, B.L., 2011. Palaeomagnetic study of the Kepezdaĝ and Yamadaĝ volcanic complexes, central Turkey: Neogene tectonic escape and block definition in the central-east Anatolides. J. Geodyn. 51, 308–326. https://doi.org/10.1016/j.jog.2010.07.004
Hisarlı, Z.M., Çinku, M.C., Ustaömer, T., Keskin, M., Orbay, N., 2016. Neotectonic deformation in the Eurasia–Arabia collision zone, the East Anatolian Plateau, E Turkey: evidence from palaeomagnetic study of Neogene–Quaternary volcanic rocks. Int. J. Earth Sci. https://doi.org/10.1007/s00531-015-1245-4
Hubert-Ferrari, A., Armijo, R., King, G., Meyer, B., Barka, A., 2002. Morphology, displacement, and slip rates along the North Anatolian Fault, Turkey. J. Geophys. Res. 107, 2235, doi ;10.1029/2001JB000393.
Hüsing, S.K., Zachariasse, W.J., van Hinsbergen, D.J.J., Krijgsman, W., Inceöz, M., Harzhauser, M., Mandic, O., Kroh, A., 2009. Oligo-Miocene foreland basin evolution in SE Anatolia: constraints on the closure of the eastern Tethys gateway, in: van Hinsbergen, D.J.J., Edwards, M.A., Govers, R. (Eds.), Geodynamics of Collision and Collapse at the Africa-Arabia-Eurasia Subduction Zone: Geological Society, London, Special Publication. pp. 107–132.
Işıker, A.K., 2002. Geological map of Turkey, scale 1:500,000, Ankara Sheet. Ankara.
Kaymakcı, N., Aldanmaz, E., Langereis, C., Spell, T.L., Gurer, O.F., Zanetti, K.A., 2007. Late Miocene transcurrent tectonics in NW Turkey: evidence from palaeomagnetism and 40Ar-39Ar dating of alkaline volcanic rocks. Geol. Mag. 144, 379.

Kaymakcı, N., Duermeijer, C.E., Langereis, C., White, S.H., Van Dijk, P.M., 2003a. Palaeomagnetic evolution of the Çankiri Basin (central Anatolia, Turkey): Implications for oroclinal bending due to indentation. Geol. Mag. https://doi.org/10.1017/S001675680300757X

Kaymakcı, N., Langereis, C., Özkaptan, M., Özacar, A.A., Gülyüz, E., Uzel, B., Sözbilir, H., 2018. Paleomagnetic evidence for upper plate response to a STEP fault, SW Anatolia. Earth Planet. Sci. Lett. 498. https://doi.org/10.1016/j.epsl.2018.06.022

Kaymakcı, N., Özçelik, Y., White, H.S., Van Dijk, P.M., 2001. Neogene tectonic development of the Çankırı basin (Central Anatolia, Türkiye). Turkish Assoc. Pet. Geol. Bull. 13, 27–56.

Kaymakcı, N., Özçelik, Y., White, S.H., Van Dijk, P.M., 2009. Tectono-stratigraphy of the Çankırı Basin: late Cretaceous to early Miocene evolution of the Neotethyan suture zone in Turkey. Geol. Soc. London, Spec. Publ. 311, 67–106.

Kaymakcı, N., White, S.H., Vandijk, P.M., 2003b. Kinematic and structural development of the Cankiri Basin (Central Anatolia, Turkey): A paleostress inversion study. Tectonophysics 364, 85–113.

Kirschvink, J.L., 1980. The least-squares line and plane and the analysis of palaeomagnetic data. Geophys. J. R. Astrol. Soc. 62, 699–718.

Kissel, C., Averbuch, O., Frizon de Lamotte, D., Monod, O., Allerton, S., 1993. First paleomagnetic evidence for a post-Eocene clockwise rotation of the Western Taurides thrust belt east of the Isparta reentrant (Southwestern Turkey). Earth Planet. Sci. Lett. 117, 1–14.

Kissel, C., Laj, C., Poisson, A., Görür, N., 2003. Paleomagnetic reconstruction of the Cenozoic evolution of the Eastern Mediterranean. Tectonophysics 362, 199--217.

Kissel, C., Laj, C., Sengör, A.M.C., Poisson, A., 1987. Paleomagnetic evidence for rotation in opposite senses of adjacent blocks in northeastern Aegean and western Anatolia. Geophys. Res. Lett. 14, 907–910.

Koç, A., van Hinsbergen, D.J.J., Kaymakci, N., Langereis, C.G., 2016. Late Neogene oroclinal bending in the central Taurides: A record of terminal eastward subduction in southern Turkey? Earth Planet. Sci. Lett. 434, 75–90. https://doi.org/10.1016/J.EPSL.2015.11.020

Koçbulut, F., Akpınar, Z., Tatar, O., Piper, J.D.A., Roberts, A.P., 2013. Palaeomagnetic study of the Karacadağ Volcanic Complex, SE Turkey: monitoring Neogene anticlockwise rotation of the Arabian Plate. Tectonophysics 608, 1007–1024.

Koçyigit, A., 1991. An example of an accretionary forearc basin from northern Central Anatolia and its implications for the history of subduction of Neo-Tethys in Turkey. Geol. Soc. Am. Bull. 103, 22–36.

Koçyiğit, A., Türkmenoğlu, A., Beyhan, A., Kaymakçı, N., Akyol, E., 1995. Post-collisional tectonics of Eskişehir-Ankara-Çankırı segment of İzmir-Ankara-Erzincan suture zone (IAESZ): Ankara orogenic phase. Türkiye Pet. Jeologları Derneği Bülteni 6, 69–86.

Koymans, M.R., Langereis, C.G., Pastor-Galán, D., van Hinsbergen, D.J.J., 2016. Paleomagnetism.org: An online multi-platform open source environment for paleomagnetic data analysis. Comput. Geosci. 93, 127–137. https://doi.org/10.1016/j.cageo.2016.05.007

Le Pichon, X., Angelier, J., 1979. The Hellenic arc and trench system: a key to the neotectonic evolution of the Eastern Mediterranean area. Tectonophysics 60, 1–42.

Lefebvre, C., Meijers, M.J.M., Kaymakcı, N., Peynircioğlu, A., Langereis, C.G., Van Hinsbergen, D.J.J., 2013. Reconstructing the geometry of central Anatolia during the late Cretaceous: Large-scale Cenozoic rotations and deformation between the Pontides and Taurides. Earth Planet. Sci. Lett. 366, 83–98.

Lucifora, S., Cifelli, F., Rojay, F.B., Mattei, M., 2013. Paleomagnetic rotations in the Late Miocene sequence from the Çankırı Basin (Central Anatolia, Turkey): The role of strike-slip tectonics. Turkish J. Earth Sci. 22, 778–792. https://doi.org/10.3906/yer-1207-2

McFadden, P.L., McElhinny, M.W., 1988. The combined analysis of remagnetisation circles and direct observations in paleomagnetism. Earth Planet. Sci. Lett. 87, 161–172.

Meijers, M.J.M., Kaymakcı, N., van Hinsbergen, D.J.J., Langereis, C.G., Stephenson, R.A., Hippolyte, J.C., 2010. Late Cretaceous to Paleocene oroclinal bending in the central Pontides (Turkey). Tectonics. https://doi.org/10.1029/2009TC002620

Mullender, T.A.T., Frederichs, T., Hilgenfeldt, C., Groot, L.V. de, Fabian, K., Dekkers, M.J., 2016. Automated paleomagnetic and rock magnetic data acquisition with an in-line horizontal "'2G"' system. Geochemistry Geophys. Geosystems 17, 2825–2834. https://doi.org/10.1002/2016GC006406

Mullender, T.A.T., Velzen, Aj., Dekkers, M.J., 1993. Continuous drift correction and separate identification of ferrimagnetic and paramagnetic contributions in thermomagnetic runs. Geophys. J. Int. 114, 663–672.

Özçep, F., 2010. Paleomagnetic studies on Anatolian plate and some geodynamic implications. Sci. Res. Essays.

Özkaptan, M., Gülyüz, E., 2019. Relationship between the anisotropy of magnetic susceptibility and development of the Haymana Anticline, Central Anatolia (Turkey). Turkish J. Earth Sci. 28, 103–121.

Özkaptan, M., Kaymakci, N., Langereis, C.G., Gülyüz, E., Arda Özacar, A., Uzel, B., Sözbilir, H., 2018. Age and kinematics of the Burdur Basin: Inferences for the existence of the Fethiye Burdur Fault Zone in SW Anatolia (Turkey). Tectonophysics 744. https://doi.org/10.1016/j.tecto.2018.07.009

Özkaptan, M., Koç, A., Lefebvre, C., Gülyüz, E., Uzel, B., Kaymakcı, N., Langereis, C.G., Özacar, A.A., Sözbilir, H., 2014. Kinematics of SW Anatolia implications on crustal deformation above slab tear, in: EGU General Assembly Conference Abstracts. p. 6061.

Özsayın, E., Dirik, K., 2007. Quaternary Activity of the Cihanbeyli and Yeniceoba Fault Zones: Inonu-Eskiflehir Fault System, Central Anatolia. Turkish J. Earth Sci. 16, 471–492.

Pastor-Galán, D., Mulchrone, K.F., Koymans, M.R., van Hinsbergen, D.J.J., Langereis, C.G., 2017. Bootstrapped total least squares orocline test: A robust method to quantify vertical-axis rotation patterns in orogens, with examples from the Cantabrian and Aegean oroclines. Lithosphere 9, 499–511.

Piper, J.D. a., Tatar, O., Gürsoy, H., 1997. Deformational behaviour of continental lithosphere deduced from block rotations across the North Anatolian fault zone in Turkey. Earth Planet. Sci. Lett. https://doi.org/10.1016/S0012-821X(97)00103-9

Piper, J.D.A., Gürsoy, H., Tatar, O., Beck, M.E., Rao, A., Koçbulut, F., Mesci, B.L., 2010. Distributed neotectonic deformation in the Anatolides of Turkey: A palaeomagnetic analysis. Tectonophysics 488, 31–50. https://doi.org/10.1016/j.tecto.2009.05.026

Piper, J.D.A., Moore, J.M., Tatar, O., Gürsoy, H., Park, R.G., 1996. Palaeomagnetic study of crustal deformation across an intracontinental transform: the North Anatolian Fault Zone in Northern Turkey, in: Morris, A., Tarling, D.H. (Eds.), Palaeomagnetism and Tectonics of the Mediterranean Region. Geological Society of London Special Publication, pp. 299–310.

Platzman, E.S., Tapirdamaz, C., Sanver, M., 1998. Neogene anticlockwise rotation of Anatolia (Turkey): preliminary palaeomagnetic and geochronological results. Tectonophysics 299, 175–189.

Reilinger, R., McClusky, S., Vernant, P., Lawrence, S., Ergintav, S., Cakmak, R., Nadariya, M., Hahubia, G., Mahmoud, S., Sakr, K., ArRajehi, A., Paradissis, D., Al-Aydrus, A., Prilepin, M., Guseva, T., Evren, E., Dmitritsa, A., Filikov, S. V, Gomes, F., Al-Ghazzi, R., Karam, G., 2006. GPS constraints on continental deformation in the Africa-Arabia-Eurasia continental collision zone and implications for the dynamics of plate interactions. J. Geophys. Res. 111, V05411, doi:10.1029/2005JB004051.

Rojay, B., 2013. Tectonic evolution of the Cretaceous Ankara Ophiolitic Mélange during the Late Cretaceous to pre-Miocene interval in Central Anatolia, Turkey. J. Geodyn. 65, 66–81. https://doi.org/10.1016/j.jog.2012.06.006

Saraç, G., 2003. Türkiye omurgalı fosil yatakları. Sci. Rep.

Şengör, A.M.., Tüysüz, O., İmren, C., Sakınç, M., Eyidoğan, H., Görür, N., Le Pichon, X., Rangin, C., 2005. the North Anatolian Fault: a New Look. Annu. Rev. Earth Planet. Sci. 33, 37–112. https://doi.org/10.1146/annurev.earth.32.101802.120415

Şengör, A.M.C., Görür, N., Şaroğlu, F., 1985. Strike-slip faulting and related basin formation in zones of tectonic escape: Turkey as a case study, in: Biddle, K.T., Christie-Blick, N. (Eds.), Basin Formation and Sedimentation. Society of Economic Paleontologists and Mineralogists Special Publications, pp. 227–264.

Sözbilir, H., 2005. Oligo-Miocene extension in the Lycian orogen: evidence from the Lycian molasse basin, SW Turkey. Geodin. Acta 18, 255–282. https://doi.org/10.3166/ga.18.255-282

Tankut, A., Güleç, N., Wilson, M., Toprak, V., Savaşçın, Y., Akıman, O., 1999. Alkali basalts from the Galatia volcanic complex, NW Central Anatolia, Turkey. Turkish J. Earth Sci. 7, 269–274.

Tatar, O., Piper, J.D.A., Park, R.G., Gürsoy, H., 1995. Palaeomagnetic study of block rotations in the Niksar overlap region of the North Anatolian Fault Zone, central Turkey. Tectonophysics 244, 251–266.

Tauxe, L., 2010. Essentials of paleomagnetism. Univ of California Press.

Toprak, V., 1998. Vent distribution and its relation to regional tectonics, Cappadocian Volcanics, Turkey. J. Volcanol. Geotherm. Res. 85, 55–67.

Toprak, V., 1994. Central Kızılırmak Fault Zone: Northern margin of Central Anatolian Volcanics. Turkish J. Earth Sci. 3, 29–38.

Uzel, B., Kuiper, K., Sözbilir, H., Kaymakci, N., Langereis, C.G., Boehm, K., 2020. Miocene geochronology and stratigraphy of western Anatolia: Insights from new Ar/Ar dataset. Lithos 352, 105305.

Uzel, B., Langereis, C.G., Kaymakci, N., Sözbilir, H., Özkaymak, Ç., Özkaptan, M., 2015. Paleomagnetic evidence for an inverse rotation history of Western Anatolia during the exhumation of Menderes core complex. Earth Planet. Sci. Lett. 414, 108–125.

Uzel, B., Sümer, Ö., Özkaptan, M., Özkaymak, Ç., Kuiper, K., Sözbilir, H., Kaymakci, N., İnci, U., Langereis, C.G., 2017. Palaeomagnetic and geochronological evidence for a major middle miocene unconformity in Söke Basin (western Anatolia) and its tectonic implications for the Aegean region. J. Geol. Soc. London. 174. https://doi.org/10.1144/jgs2016-006

van Hinsbergen, D.J.J., Kaymakcı, N., Spakman, W., Torsvik, T.H., 2010. Reconciling the geological history of western Turkey with plate circuits and mantle tomography. Earth Planet. Sci. Lett. 297, 674–686.

van Hinsbergen, D.J.J., Langereis, C.G., Meulenkamp, J.E., 2005. Revision of the timing,

magnitude and distribution of Neogene rotations in the western Aegean region. Tectonophysics 396, 1–34.

van Hinsbergen, D.J.J., Maffione, M., Plunder, A., Kaymakcı, N., Ganerød, M., Hendriks, B.W.H., Corfu, F., Gürer, D., Gelder, G.I.N.O., Peters, K., 2016. Tectonic evolution and paleogeography of the Kırşehir Block and the Central Anatolian Ophiolites, Turkey. Tectonics 35, 983–1014.

Van Velzen, A.J., Zijderveld, J.D.A., 1995. Effects of weathering on single domain magnetite in early Pliocene marls. Geophys. J. Int. 267–278.

Vasiliev, I., Franke, C., Meeldijk, J.D., Dekkers, M.J., Langereis, C.G., Krijgsman, W., 2008. Putative Greigite Magnetofossils From The Pliocene Epoch. Nat. Geosci. 1, 782–786. https://doi.org/10.1038/ngeo335

Wilson, M., Tankut, A., Guleç, N., 1997. Tertiary volcanism of the Galatia province, north-west Central Anatolia, Turkey. Lithos 42, 105–121.

Zijderveld, J.D.A., 1967. A.c. demagnetisation of rocks: analysis of results, in: Collinson, D.W., al., et (Eds.), Methods in Palaeomagnetism. Elsevier, Amsterdam, pp. 254–286.